IOP Publishing

The Structure of Amorphous Materials using Molecular Dynamics

Carlo Massobrio

Chapter 6

The atomic structure of disordered networks

Disordered $GeSe_2$ systems have been identified as prototype networks made of a predominant tetrahedral motif coexisting with miscoordinations and homopolar bonds. The pattern exhibited by the pair correlation functions and the partial structure factors is far from trivial, calling for quantitative models to be employed and carefully tested so as to ascertain their performances. In this chapter, we begin to report on first-principles molecular dynamics (FPMD) calculations on disordered chalcogenides by focusing on liquid and glassy $GeSe_2$. We describe first their structural properties, by showing that the agreement with experiments is unequal for the Ge and Se and it is particularly challenging for the Ge environment. As a second issue, we take advantage of the existence of intermediate range order in these networks to reconsider available interpretations for the origin of the first-sharp diffraction peak (FSDP) in the total and in the concentration–concentration structure factor $S_{CC}(k)$. At both levels (total and partial structure factors), we proposed two atomic-scale interpretations for the origins of this feature. A further section is devoted to the comparison, for different glassy systems, between the charge–charge structure factor $S_{zz}(k)$ and $S_{CC}(k)$. This allows extracting a criterion linking the presence of the FSDP to the topology of the network. Also, the concept of charge neutrality is rationalized. As a final item of this chapter, we show how the quest of improvements in the description of prototypical disordered chalcogenides brings us to the choice of a specific exchange–correlation (XC) functional (BLYP, introduced in section 4.2.1), able to enhance electronic localization.

6.1 General consideration: where do we start from?

There are several ways of getting interested in disordered materials from the theoretical viewpoint. One consists in focusing on a given property, feature and/or specific mark or pattern that shows up in a class of systems by attempting to understand its origin and what makes it so special for those materials. By using molecular dynamics (MD), the fact of working at the atomic-scale drives the search of

doi:10.1088/978-0-7503-2436-6ch6

all possible connections between what we are able to observe (experimental data) and the relationship with microscopic quantities accessible to the atomic-scale observation, that is to say the variable for which we can calculate a statistical average. Focusing on a specific property and on its peculiarities has the advantage of stimulating curiosity for other physical and chemical features of the targeted systems, by nurturing a rewarding approach to more extended knowledge. These considerations apply to the road of discovery that will be detailed here for chalcogenides, the class of disordered network-forming systems mostly invoked in the part of this monograph. When we started working on these systems, the key quantities attracting attention for its intriguing behavior and the implications on the atomic-scale description of disordered systems (liquids and glasses) were the partial structure factors. In particular, a feature developing at short values (typically 1 $Å^{-1}$) of the momentum transfer in reciprocal space was the object of investigations, namely the so-called first-sharp diffraction peak (FSDP) [1], indicative of intermediate range order developing on distances substantially longer than the nearest neighbors. As a feature appearing in many different systems, the FSDP was both considered a quantity to be interpreted on the basis of generic models and a signature of specific network topologies deserving accurate treatment (at the first-principles level) of chemical bonding. Our approach was mostly of the second kind, even though we had to acknowledge that there is a lot to learn on FSDP and IRO (intermediate range order) with interatomic potentials.

In what follows, we shall focus on liquid and glassy $GeSe_2$ as prototype systems to understand the interplay between atomic structure, level of the description of the potential energy surface and intermediate range order. The consideration of a liquid is part of a general analysis involving disordered network-forming systems, all ideas developed thereof applying equally well to glasses. For comparative purposes, other systems will be also touched upon, although much less extensively. When discussing the main features of the classical MD potentials in section 3.3, we mentioned that the ionic approximation inherent in equations (3.13) and (3.14) could not account for the presence of homopolar bonds in disordered $GeSe_2$. From a strictly historical perspective, it should be said that stringent evidence on the presence of homopolar bonds was not available when the results on disordered $GeSe_2$ were published, this factor contributing to their highest recognition. In addition, the total neutron structure factor was in good agreement with experiments, with the inclusion of the FSDP. While the availability of partial structure factors and the related pair correlation functions pointed out the deficiencies we referred to in section 3.3, there is a more profound reason marking the inability of point-charge potential models to compare realistically with diffraction experiments. In references [2–4] two statements were put forth, the *first* highly valuable and interesting, the *second* equally valuable but revealing of an excessive simplification in terms of chemical bonding built in the potential itself.

1. The *first* statement amounts to attributing the appearance of the FSDP to a combination of steric and charge effects, a simple charged sphere models allowing for these conditions to be met. In this way, one is able to rationalize the very good behavior of the potential when employed to reproduce the total neutron structure factor and, in real space, to promote a tetrahedral network made of connected tetrahedra, a general topological feature well accepted ever

since early experiments were made available. Note that in this context the potential based on point charges can be considered a refinement of the charged sphere models, by equally promoting the establishment of a tetrahedral network and the presence of a FSDP.

2. The *second* statements issued by references [2–4] has to do with the absence of the FSDP in the charge–charge structure factor $S_{zz}(k)$, that becomes trivially proportional to the concentration–concentration structure factor $S_{CC}(k)$ (defined in equation (2.6)) for a purely ionic system made of point charges. This was proposed to be a universal property of binary AX_2 disordered systems, by virtually ruling out any fluctuations of concentration and of charge on intermediate range distances, since for the point-charge model $S_{zz}(k)$ and $S_{CC}(k)$ are essentially equal (proportional).
3. Given this situation, one is faced with the dilemma of disproving (or confirming) that ionic models are sufficiently accurate for disordered chalcogenides by collecting any possible evidence (from experiments and/or theory) on the behavior of $S_{CC}(k)$. Therefore, our first goal was to describe liquid (and glassy) $GeSe_2$ system in the framework of FPMD and obtain properties in real and reciprocal space to be compared with experiments. This is where the partial structure factors measured by the team of P Salmon via isotopic substitution in neutron diffraction come into play [5, 6] since both investigations on the glassy and liquid $GeSe_2$ showed a clear FSDP in $S_{CC}(k)$, thereby opening an intense line of study that has marked our engagement in the area of disordered network-forming material for many years.

In what follows, we shall focus on the following issues in different sections of this chapter.

1. We describe first the structural properties of liquid and glassy $GeSe_2$, by pointing out the level of agreement with experiments and the issues left open at the time the calculations were carried out.
2. As a second point, we take advantage of the availability of FPMD calculation for several systems to discuss existing interpretations for the origin of the first-sharp diffraction peak in the total structure factor. This analysis is extended to the presence of the FSDP in the concentration–concentration structure factor, for which we achieved a substantial breakthrough by linking the FSDP to a specific structural motif.
3. As a third point, we carry out a comparative analysis of the charge–charge and concentration–concentration structure factors $S_{zz}(k)$ and $S_{CC}(k)$, leading to a general criterion for the appearance of intermediate range order based on the concept of charge neutrality at the appropriate scales.
4. We have devoted section 3.6.5 to the role played by the generalized gradient approximation (GGA) (the one by Perdew and Wang in that case) to obtain realistic structural properties for liquid $GeSe_2$. That result was at the origin of our decision to pursue the study of disordered chalcogenides by relying on GGA calculations. Here we look for further improvements by considering an alternative XC functional (BLYP, introduced in section 4.2.1), by showing that this choice brings the calculations in better agreement with experiments for certain properties, especially those pertaining to the Ge subnetwork.

6.2 The structure of liquid and glassy $GeSe_2$

6.2.1 Methodology

Here we shall focus on the FPMD model based on the PW exchange–correlation functional, by referring mostly to reference [7] for the liquid case and to reference [8] for the glassy case. These calculations share the same technical features and were published at a 7 years interval, partially because it was decided to collect much more statistics for the glassy case. In terms of technical tools, we are referring here to a plane wave code running on vectorial computers (essentially the one developed by Alfredo Pasquarello and Roberto Car at EPFL Lausanne in the 1990s) and on grants quite limited on a yearly basis, this situation imposing some limitations on the size of the system and on the temporal trajectories. Also, this explains why it took quite some time to obtain several trajectories for the glass. Parallel computers were already available at the beginning of the century but the CPMD code was not yet exploited with its parallel implementation for the cases considered here. When facing the size and time issues of the plane waves/pseudopotential scheme within FPMD, any size larger than ~150–200 atoms was unaffordable at those times, our first results based on larger sizes (say, ~500 atoms) becoming available later, after the year 2010. Given the performances of those computers, included the largest ones running on national facilities, there was no point in hoping to circumvent the strong non-linear behavior with size of the Kohn–Sham Hamiltonian, for which we recorded at that time a cost about one hundred times more important when going from $N_{at} = 100$ to $N_{at} = 500$.

- Technically speaking, it is legitimate to work with $N_{at} = 120$ to get information on intermediate range order, given the smallest wave vector compatible with the periodic cell, $k_{min} = 0.5$ Å^{-1}, smaller than the FSDP wave vector $k_{FSDP} = 1$ Å^{-1}, with as many as eight discrete k values describing the region of wave vectors around the FSDP. For these reasons, the need to switch to a larger system appeared less acute and could be postponed without sacrificing (at least as much as we could at that time) the quality of our achievements.
- As to the issue of the length of the trajectory, our strategy consisted in working with the largest time step compatible with a good energy conservation (about 0.5 fs, 20 a.u.), even though this choice appears today a bit risky in terms of adiabaticity since corresponding to fairly large values of the fictitious mass for the electronic degrees of freedom μ (5000 a.u.). Careful use and tuning of the Nosé–Hoover thermostats (see section 3.5.5) have granted success to these simulations, regardless of the fact that working with smaller time step and μ would have been much more costly but safer. For the liquid, equilibrium trajectory lasted ~20 ps, a value allowing for calculation of sensible average properties due to the effective sampling of the phase space.
- For the glass, a typical quench schedule was the one described in section 4.4.5, where we stressed the importance of following the behavior of some quantities in time before considering them as stationary property. This consideration proved valuable even in the case of quench rates faster than 10^{13} K s^{-1}. In the case of the glass, we produced $N_{tr} = 6$ trajectories by considering the average properties obtained from each trajectory as partial averages contributing to a

global one (the mean value). The error bar attributed to the mean value is taken to be $\sigma_{\text{mean}} = \sigma/\sqrt{N_{\text{tr}} - 1}$ where σ is is half the largest difference among the N_{tr} partial averages.

6.2.2 Liquid $GeSe_2$

As a first information on the structure (and the extent of intermediate range order) of liquid $GeSe_2$ we can focus on the Faber–Ziman (FZ) [9] partial structure factors (figure 6.1), introduced in section 2.3[1].

Focusing on $S_{\text{GeGe}}(k)$, the main difference between neutron scattering experiments [6] and our calculations is found at the FSDP level, with a much lower

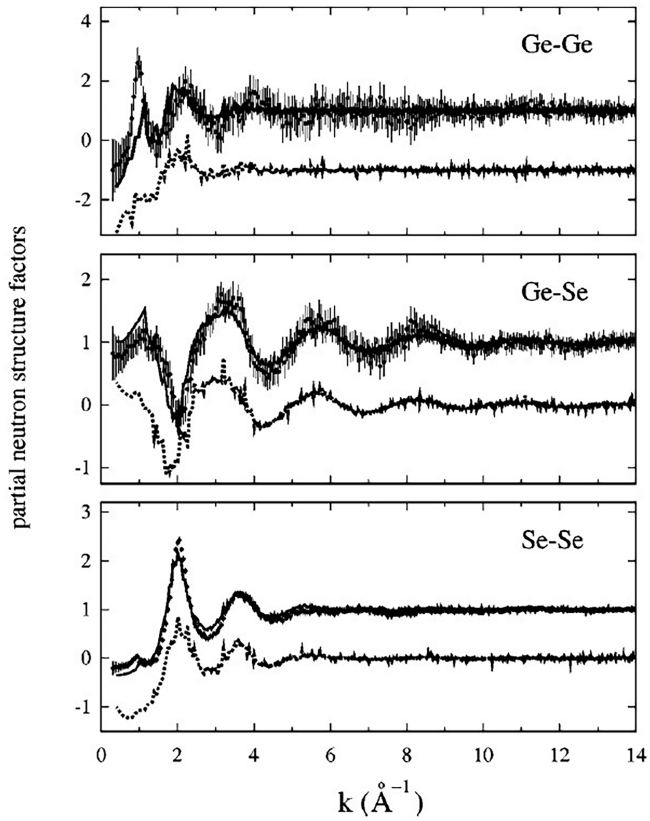

Figure 6.1. Partial structure factors for liquid $GeSe_2$: solid line: PW-GGA calculations; dotted line: LDA calculations; dots with error bars: experiments [6]. LDA results have been shifted down by 2, 1, and 1, respectively. Reprinted figure with permission from [7]. Copyright (2001) by the American Physical Society.

[1] From now on we shall drop the label FZ when indicating the partial structure factors, unless when using explicitly the Bhatia–Thornton (BT) [10, 11] partial structure factors as introduced in section 6.3. Also, we shall not comment on local density approximation (LDA) results since the limited performances of these calculations have been already highlighted previously (see section 3.6.5).

intensity in the CPMD result. This holds true even when accounting for error bars of the FSDP, estimated by taking partial averages on time periods of 2 ps and amounting to as much as 20%. This high value is mostly due to the size of our system (with as little as 40 Ge atoms) and it expresses strong fluctuations in the intermediate range properties. We shall exploit this variability when analyzing the correlation between the FSDP in $S_{CC}(k)$ and specific structural motifs (see section 6.3.2). Despite some small, discernible differences, theory is in much better agreement with experiments for the case of $S_{GeSe}(k)$ and $S_{SeSe}(k)$. This provides a first indication of a general feature of disordered Ge–Se systems modeled by FPMD (Ge–Ge correlations somewhat more problematic than Se–Se and Ge–Se ones) that will be observed throughout our studies.

It is of interest to see (figure 6.2) how this fact is reflected by the behavior of the Bhatia–Thornton [10] partial structure factors $S_{NN}(k)$ (number–number), $S_{NC}(k)$ (number–concentration) and $S_{CC}(k)$ (concentration–concentration), introduced in section 6.3, where we pointed out that for the $GeSe_2$ composition $S_{NN}(k)$ is a very

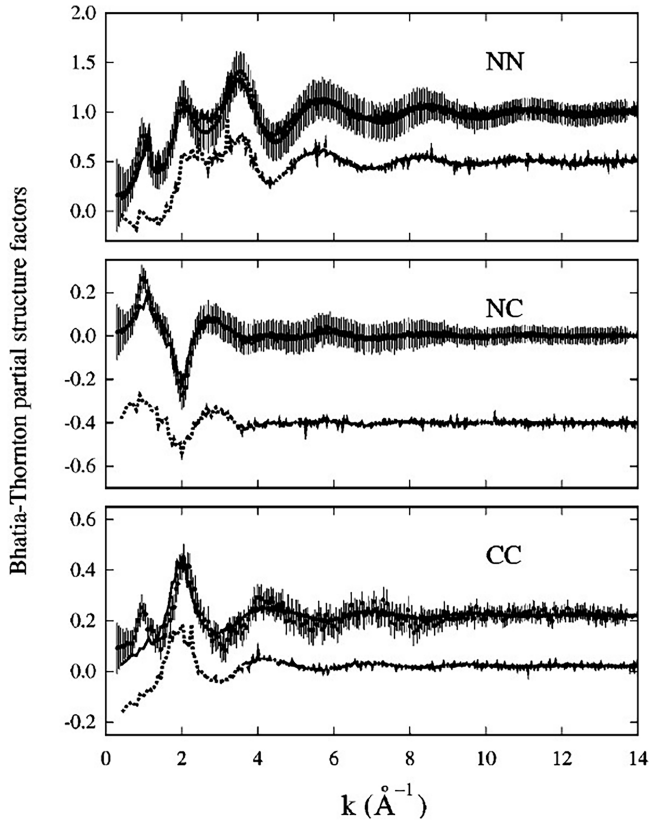

Figure 6.2. The Bhatia–Thornton partial structure factors for liquid $GeSe_2$: PW-GGA calculations: solid line; LDA calculations: dotted line; experiments: dots with error bars, [11]. LDA results have been shifted down by 0.5, 0.4, and 0.2, respectively. Reprinted figure with permission from [7]. Copyright (2001) by the American Physical Society.

good approximation of the total neutron structure factor $S_T(k)$. Both $S_{NN}(k)$ and to a smaller extent $S_{NC}(k)$ agrees very well with experiments for the entire k range, while in the case of $S_{CC}(k)$ experiments are reproduced only for $k > 1.5$ Å^{-1}. It appears that the very prominent FSDP observed experimentally is absent in the theoretical $S_{CC}^{GGA}(k)$, this difference showing that, overall, the comparison between experimental and theoretical partial structure factors is highly favorable for k values characteristic of short-range properties ($k > 2$ Å^{-1}). However, the FSDP weights in the partial structure factors are distributed differently in theory and experiment. This difference manifests itself through the behavior of $S_{GeGe}(k)$ and (very moderately) of $S_{GeSe}(k)$. Quite intriguingly these discrepancies tend to cancel with each other in the total structure factor, while they concur to produce a clear deviation at the FSDP position in $S_{CC}(k)$.

Focusing on the properties in real space through the analysis of the pair correlation functions $g_{\alpha\beta}(r)$, compared to experiments [6] in figure 6.3, unequal performances are recorded for $g_{GeGe}(r)$, $g_{GeSe}(r)$ and $g_{SeSe}(r)$. These are quantified through the positions of the main peaks and the number of neighbors as given in

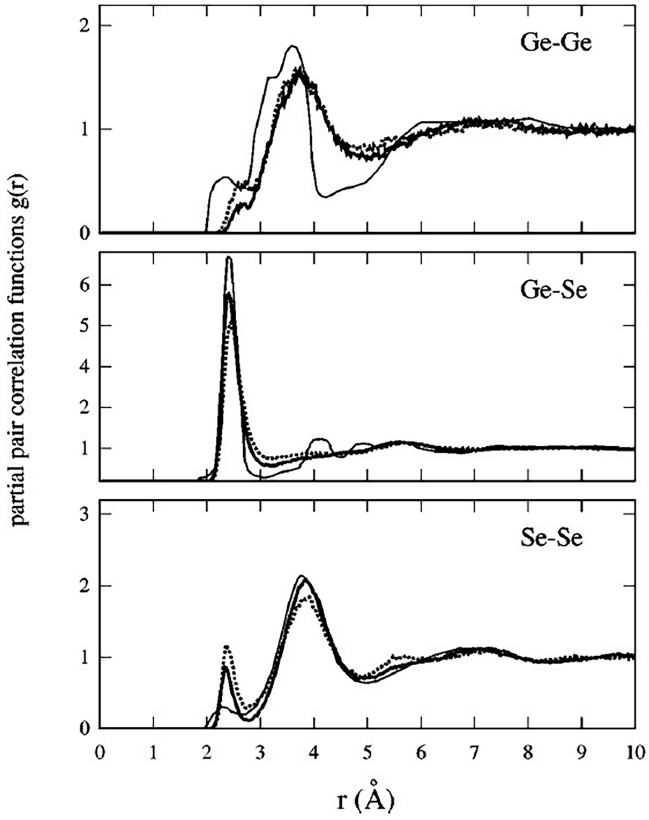

Figure 6.3. Partial pair correlation functions for liquid $GeSe_2$: PW-GGA calculations: thick line; LDA calculations: dotted line; experiments: solid line, [6]. Reprinted figure with permission from [7]. Copyright (2001) by the American Physical Society.

table 6.1. Partial pair correlations $g_{GeSe}(r)$ and $g_{SeSe}(r)$ are consistent with experiments, with close values for the first neighbors coordination shells numbers n_{Ge}^{Se} and n_{Se}^{Se}. Larger differences are found in the case of $g_{GeGe}(r)$. Experiments exhibit a clear distinction between shells of neighbors, with first maximum and minimum. Theory appears to smooth out the relevant peaks and minima, leading to a description of the Ge–Ge environment virtually resembling a behavior at higher temperatures.

There are fewer homopolar bonds than in experiments and, additionally, they are found at larger distances as indicated by n_{Ge}^{Ge} in table 6.1. In [7] it was pointed out that longer interatomic Ge–Ge distances and less structured Ge–Ge pair correlation functions were found in liquid GeSe within the same theoretical framework [12]. Since such longer Ge–Ge bond lengths are typical of the metallic liquid Ge, we obtain a strong indication of the overestimate of the metallic bonding in liquid $GeSe_2$. Overall, results in reciprocal and real space have a twofold character and can be commented upon by underlying both positive and less satisfactory features. On the positive side, FPMD with Perdew–Wang GGA proved able to achieve a very good agreement with neutron scattering experiments, including the presence of homopolar bonds (not accessible to any interatomic potential at that temperature) and the appearance of the FSDP. This can be considered as a success of our approach, validating a detailed analysis of the structural motifs contained in the network. Less favorable is the description of Ge–Ge correlations, both at short and intermediate range distances. Ever since the production of these results, this shortcoming has been a strong motivation to improve the atomic-scale description in two directions, namely the consideration of other XC schemes and the study of size effects. While the Perdew–Wang GGA scheme remains a valuable choice, the overestimate of Ge–Ge bond lengths together with the flattened shape of $g_{GeGe}(r)$ were strong indication of a still insufficient account of the ionic character of bonding. Looking for a size effect was also a quite natural option, while falling into the category of effect quite hard to control in an exhaustive manner, macroscopic dimension being in any case inaccessible. Further details on these issues will be given elsewhere in this book (see chapter 9).

Table 6.1. First (FPP) and second (SPP) peak positions in experimental [6] and theoretical $g_{\alpha\beta}(r)$ [7]. The integration ranges corresponding to the coordination numbers n_α^β and m_α^β are 0–2.6 Å, 2.6–4.2 Å for $g_{GeGe}(r)$, 0–3.1 Å, 3.1–4.5 Å for $g_{GeSe}(r)$ and 0–2.7 Å, 2.7–4.8 Å for $g_{SeSe}(r)$. Error bars are the standard deviations from the mean for subaverages of 2 ps. Reprinted table with permission from [7]. Copyright (2001) by the American Physical Society.

$g_{\alpha\beta}(r)$	FPP (Å)	n_α^β	SPP (Å)	m_α^β
$g_{GeGe}(r)$	2.7 ± 0.1	0.04 ± 0.01	3.74 ± 0.05	2.74 ± 0.06
$g_{GeGe}^{exp}(r)$	2.33 ± 0.03	0.25 ± 0.10	3.59 ± 0.02	2.9 ± 0.3
$g_{GeSe}(r)$	2.41 ± 0.10	3.76 ± 0.01	5.60 ± 0.01	3.72 ± 0.03
$g_{GeSe}^{exp}(r)$	2.42 ± 0.02	3.5 ± 0.2	4.15 ± 0.10	4.0 ± 0.3
$g_{SeSe}(r)$	2.34 ± 0.02	0.37 ± 0.01	3.84 ± 0.02	9.28 ± 0.04
$g_{SeSe}^{exp}(r)$	2.30 ± 0.02	0.23 ± 0.05	3.75 ± 0.02	9.6 ± 0.3

By taking advantage of $n_\alpha(l)$, defined as the average number of atoms of species α l-fold coordinated we can calculate the percentage of Ge and Se atoms coordinated to various units composed of l neighbors having a well defined chemical nature. This analysis reveals that fourfold coordinated atoms are predominant but limited to 61%. Chemical disorder is quantified by the presence of threefold coordinated Ge atoms (22.4%), and fivefold coordinated Ge atoms (10.8%) as well as 16.5% Ge atoms forming homopolar bonds. Similarly Se atoms are found in twofold configurations (70.3%), but 25% of them are threefold coordinated and 32% form homopolar bonds. The picture arising from these numbers corresponds to that of a network in which the tetrahedral units are by far the most frequent form of coordination among Ge and Se atoms (the $GeSe_4$ tetrahedra). However, there is a conspicuous number of miscoordinations under the form of homopolar bonds or other than fourfold (for Ge) and twofold (for Se) connections, marking the difference between a realistic FPMD model and descriptions based on point-charge interatomic potentials [2–4, 13].

6.2.3 Glassy $GeSe_2$

By following the same line of presentation than in the previous section, we consider first properties in reciprocal space. The calculated total neutron structure factor $S_T(k)$ (for which all considerations relative to its representation via $S_{NN}(k)$ hold as in the liquid case) is compared to the experimental data [14] in figure 6.4.

Once again, the very good agreement over the entire range of values is affected by the behavior for $k < 2$ Å^{-1}, with no clear minimum between the first two peaks and the FSDP of lower intensity. The origin of this disagreement can be traced back to the partial structure factor $S_{GeGe}(k)$ shown in figure 6.5 together with $S_{GeSe}(k)$ and $S_{SeSe}(k)$, for which the level of comparison is quite outstanding. Differences between theory and experiments in $S_{GeGe}(k)$ are noticeable for $k < 3$ Å^{-1}, following the same

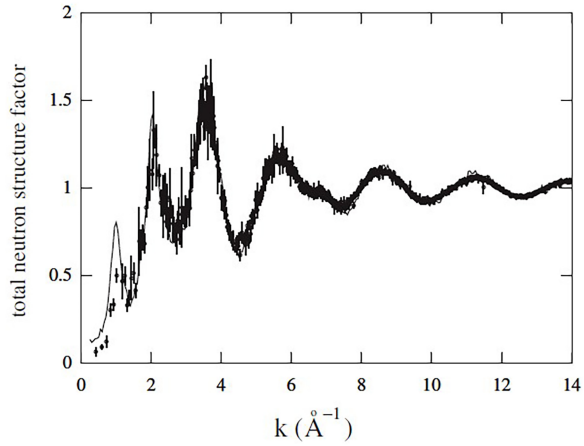

Figure 6.4. Total neutron structure factor of glassy $GeSe_2$: circles with error bars: FPMD results [8]; solid line: neutron scattering experiments [14]. Reprinted figure with permission from [8]. Copyright (2008) by the American Physical Society.

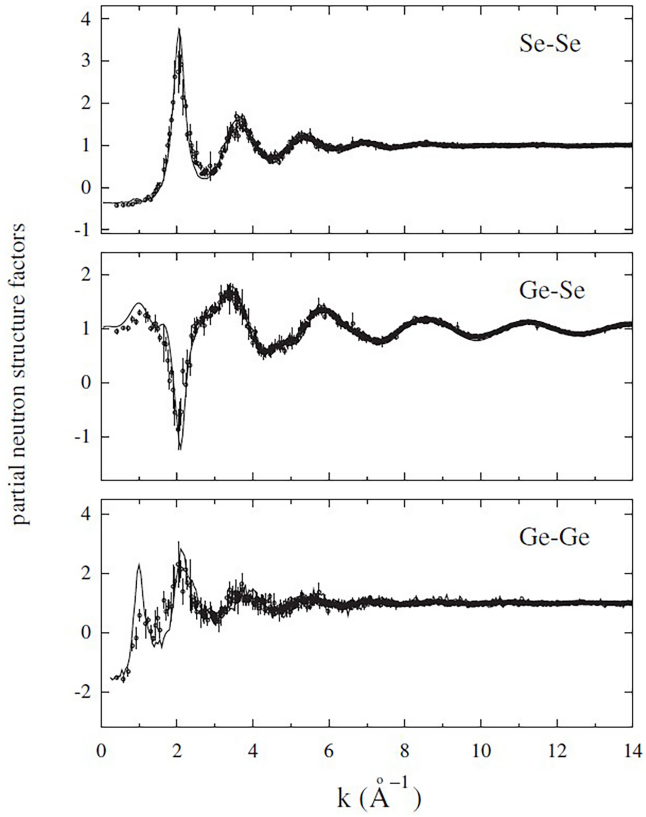

Figure 6.5. Partial structure factors of glassy $GeSe_2$: circles with error bars: FPMD results [8]; solid line: neutron scattering experiments [5]. Reprinted figure with permission from [8]. Copyright (2008) by the American Physical Society.

behavior observed for $S_T(k)$. Therefore, glassy $GeSe_2$ reproduces in reciprocal space the pattern already observed for the liquid, with a broad agreement on the intermediate range properties when it comes to Ge–Se and Se–Se correlations, this agreement worsening in the Ge–Ge case, resulting in a shape not adequately reproduced in the FSDP region.

Similar considerations hold for the case of $S_{CC}(k)$, that agrees with its experimental counterpart in the range $k \geqslant 2$ Å^{-1}, while at lower k values, the FSDP takes a shoulder shape for 1 Å^{-1} $< k <$ 1.7 Å^{-1} (figure 6.6). However, the disagreement between theory and experiments at low values of k is less severe in the glassy than in the liquid case.

When addressing the structural properties of glassy $GeSe_2$, it is worthwhile to begin our review of the results of [8] by examining $g_{GeGe}(r)$ since for $g_{SeSe}(r)$ and, to a larger extent for $g_{GeSe}(r)$, our level of theory is able to compare adequately to experiments, the few differences found in $g_{SeSe}(r)$ being almost accounted for by the error bars (see figure 6.7). The comparison between experiments and theory for $g_{GeGe}(r)$ can be based on three distinct marks in the interval 2 Å $< r <$ 4 Å. These

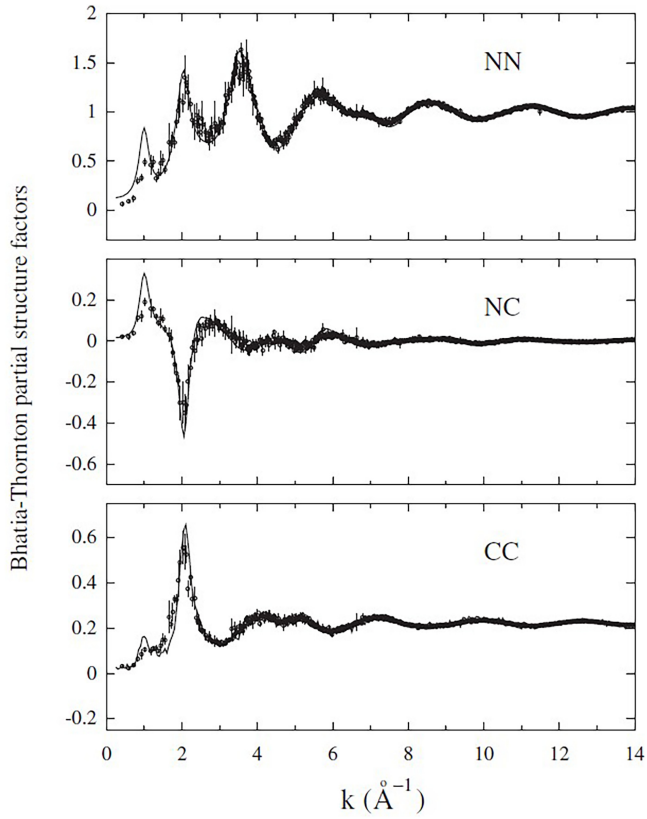

Figure 6.6. Bhatia–Thornton partial structure factors of glassy $GeSe_2$: circles with error bars: FPMD results [8]; solid line: neutron scattering experiments [5]. Reprinted figure with permission from [8]. Copyright (2008) by the American Physical Society.

correspond to homopolar Ge–Ge bonds, Ge atoms forming edge-sharing connections, and Ge atoms forming corner-sharing connections, respectively. Worthy of note is the fact that the error bars is as large as 50% in the interval 2.3 Å$<r<$2.7 Å around the first maximum of $g_{GeGe}(r)$. We are faced here with a pattern recalling the less structured profile already observed in the case of the liquid, by confirming the limits inherent in the description of Ge–Ge correlations by using the GGA-PW scheme. A first, striking consequence is the underestimate in the value of the coordination number n_{Ge}^{Ge} (0.07 ± 0.04 against 0.25 [5]).

The description of the short-range structure contained in table 6.2 is indicative of a larger number of both fourfold coordinated Ge atoms and twofold coordinated Se atoms than in the liquid ((75 ± 6)% vs 61% and (93 ± 6)% vs 70%, respectively). This means that the chemical order is partially restored upon cooling. In addition to the predominant tetrahedral coordination, Ge atoms are also found in first-neighbor shells made of of GeSe, $GeSe_2$ and $GeSe_3$. Also, homopolar Ge connections concern two Ge–Se_3 units that merge to form a Se_3–Ge–Ge–Se_3 ethane-like group. Table 6.2 confirms the coexistence of tetrahedra and chemical disorder as a peculiar feature of

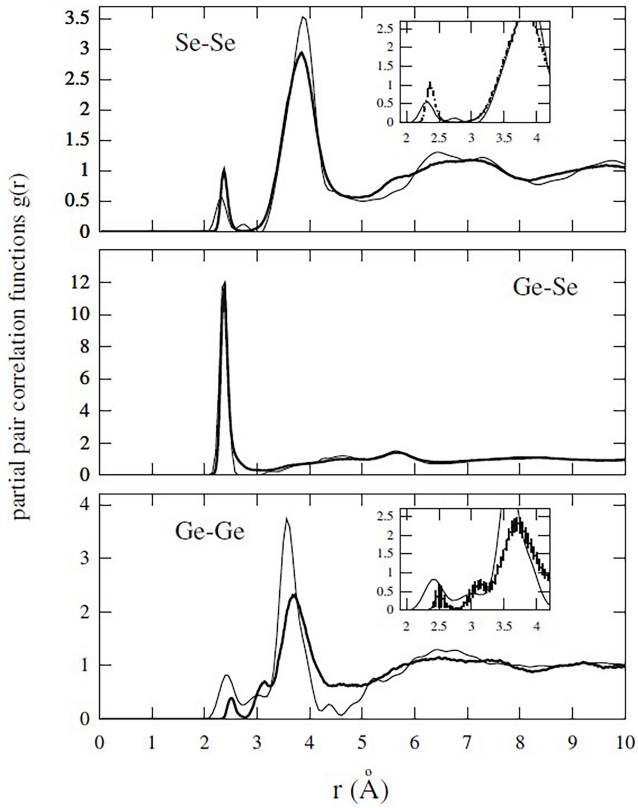

Figure 6.7. Pair correlation functions of glassy $GeSe_2$. Thick line: FPMD results, reference [8]. Thin line: neutron scattering experiments, reference [5]. In the case of $g_{GeGe}(r)$ and $g_{SeSe}(r)$, the interval of distances between 1.9 Å and 4.2 Å has been magnified in the inset and the associated error bars are shown. Reprinted figure with permission from [8]. Copyright (2008) by the American Physical Society.

chalcogenide disordered networks. Once again, from the methodological point of view, the success in reproducing most of the experimental quantities issued from structural measurements is moderately undermined by inaccuracies in the description of the environment pertaining to Ge atoms.

6.2.4 Modeling these two systems: some thoughts

When trying to summarize the main achievements contained in the investigations of glassy $GeSe_2$, the following considerations are in order. Both liquid and glassy $GeSe_2$ can be described as systems in which the tetrahedron is the main short-range structure, coexisting with homopolar bonds and miscoordinations. In the case of amorphous $GeSe_2$, several temporal trajectories have been produced, via quenches from uncorrelated configurations of the liquid. The deviation from chemical order found in the liquid (the number of defects, coordinations other than four for Ge and other than two for Se) can be reduced as a result of the cooling process, showing that high quench rates do not prevent structural change driven by the temperature

Table 6.2. Average number $n_\alpha(l)$ (expressed as a percentage) of Ge and Se atoms l-fold coordinated at a distance of 2.7 Å. For each value of $n_\alpha(l)$, we give the identity and the number of the Ge and Se neighbors. $n_\alpha(l)$ has been defined in section 2.4.1. We also compare calculated and experimental values (in percentage) for the number of Ge atoms forming edge-sharing connections, $N_{Ge}(ES)$, the number of Ge atoms forming corner-sharing connections, $N_{Ge}(CS)$, the number of Ge atoms involved in homopolar bonds, N_{Ge-Ge}, and the number of Se atoms involved in homopolar bonds, N_{Se-Se}. Experimental values are taken from [15]. Reprinted table with permission from [8]. Copyright (2008) by the American Physical Society.

Ge	$l = 1$		$l = 2$	
	Se	5 ± 1	Se_2	12 ± 1
	$l = 3$		$l = 4$	
	Se_3	8 ± 1	$GeSe_3$	5 ± 2
			Se_4	70 ± 4
Se	$l = 1$		$l = 2$	
	Ge	4 ± 1	Se_2	3 ± 1
			SeGe	21 ± 1
			Ge_2	69 ± 1
	$l = 3$			
	Ge_3	4 ± 1		
	$N_{Ge}(ES)$	$N_{Ge}(CS)$	N_{Ge-Ge}	N_{Se-Se}
Reference [8]	45 ± 4	50 ± 6	5 ± 2	24 ± 2
Experiment	34	41	25	20

reduction. FPMD is reliable and quite realistic throughout. However, its weak point resides in the treatment of Ge–Ge correlations for both liquid and glassy $GeSe_2$, as revealed by the shape of the pair correlation functions $g_{GeGe}(r)$. Knowing that the use of the GGA (in the Perdew–Wang form) was already crucial to improve improved the structural description with respect to LDA, this appeared as a good starting point in the search of alternative XC recipes capable of bringing theory in better agreement with experiments. Also, consideration of larger size could not be excluded, despite our repeated efforts to demonstrate the consistency of calculations with $N_{at} = 120$. Achievements aimed at going beyond the scheme employed for liquid and glassy $GeSe_2$ during the period 1998–2007 (PW XC functional and $N_{at} = 120$) will be the topic of section 6.7.

6.3 The origin of the first-sharp diffraction peak

6.3.1 FSDP in the total structure factor

The presence of the FSDP in the total structure factor and in some of the partial structure factors of disordered network-forming materials has stimulated intense work aimed at understanding its atomic-scale origin. In the previous sections we

have provided examples of the occurrence of this feature in liquid and glassy $GeSe_2$. By leaving aside for a moment the specific case of these systems and the review of structural properties of other chalcogenides, it is of interest to focus on a series of attempts that were made to link the FSDP to specific structural motifs.

As a first step, we concentrate on the analysis of some interpretations proposed in the literature, with the intent of assessing their general character. The team of Vashishta [4] was the first to demonstrate that the FSDP can be observed even in binary AX_2 model systems made of charged hard spheres, provided one selects appropriate values for the charges and the relative dimensions of the hard spheres, resulting in the right combination of steric and charge effects. To put it in simple, intuitive terms, this means that the FSPD comes along when the tetrahedra take over, while it tends to disappear when this main structural motif is no more predominant. This is exactly what happens in [4] when the system is neutral, approaching the random close packing, at least for Se atoms. Therefore, the appearance of the FSDP is not related to the details of the potential or, better, to details of chemical bonding, the feature being a fingerprint of a predominant structural motif. While this statement says little about the microscopic origin (since it determines merely under which condition the FSDP appears), it is useful to approach this issue from the opposite viewpoint, namely by looking for specific conditions causing the FSDP to disappear.

6.3.1.1 Learning from liquid $GeSe_2$ at high temperatures

In [16] we have compared the total neutron structure factors of liquid $GeSe_2$ at $T = 1050$ K (as shown in section 6.2.2) and at $T = 1373$ K, for which experimental data were also available. The strong decrease of the FSDP visible in figure 6.8 can be correlated to lower percentages of Ge forming $GeSe_4$ (or defective) tetrahedra, lowering to 37%. Also, the short-range chemical disorder is enhanced at higher

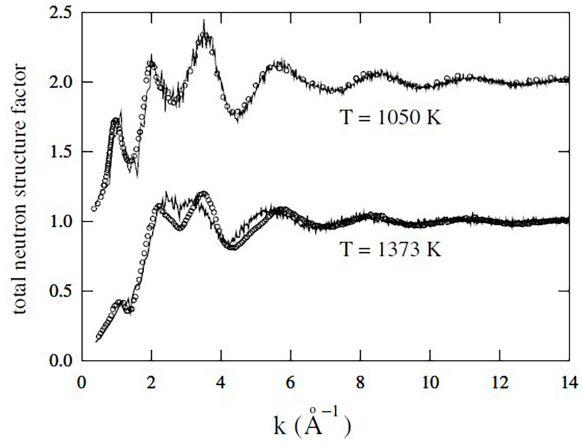

Figure 6.8. Total neutron structure factors for liquid $GeSe_2$ at $T = 1050$ K and $T = 1373$ K. Open circles: experimental results ($T = 1050$ K [6]) and ($T = 1373$ K [17]). Solid line: FPMD results ($T = 1050$ K [7]) ($T = 1373$ K [16]). Copyright (2000) courtesy IOP Publishing.

temperatures, since a larger number of coordination different than fourfold (for Ge) and twofold (for Se) are present in the network. Incidentally, it is worth mentioning that the notion of chemical order in AX_2 systems is particularly straightforward to check, since perfect chemical order corresponds to the highest number of atoms forming heterogeneous (non-homopolar) bonds.

Based on these results we are in a position to state that the FSDP (at the level of the total structure factor) shows up when there is a predominant unit accounting for more that ~50% of all structural motifs describing the coordination of atomic species. This structural motif is the tetrahedron in the case of disordered $GeSe_2$, the impact of changes in the composition being also a crucial factor to determine the structure of Ge_xSe_{1-x} networks, as it will be shown in chapter 8.

6.3.1.2 State of the art and available interpretations

Having in mind the atomic-scale origins of the FSDP, it also appropriate to check previous hypotheses advanced to rationalize the existence of correlations on length scales going beyond nearest-neighbor bond distance [18]. About 20 years ago, we started from the observation that a wide range of interpretation schemes had been made available to link the FSDP to some specific structural motifs [1–4, 18–26], by coming to the conclusion that FPMD could be instrumental to revisit two of them. The first set of interpretations can be labeled as the *layers* conjecture, since it views the FSDP as linked to some reminiscent crystalline order that manifests itself through the presence of layers. These are separated by a distance prompting the appearance of the FSDP in reciprocal space [26, 27]. While there is no reason *a priori* to look for signatures of the crystalline state in an amorphous structure beyond nearest neighbors, it should be recalled that some authors were somewhat attracted into this hypothesis by the presence of a layered structure in the corresponding crystals [22–24]. A second interpretation (termed hereafter *cluster–voids*) is based on the existence of regions having a peculiar low-density inner parts embedded in 'voids', related by distances typical of intermediate range order [18, 21].

6.3.1.3 Checking the different hypotheses

We have taken advantage of trajectories previously obtained by FPMD for liquid SiO_2 [28] and liquid $GeSe_2$ (as detailed above in section 6.2.2) at 3500 K and 1050 K, respectively. The case of liquid SiO_2 is worth commenting on briefly, since it corresponds to a disordered network chemically ordered with very few defects, unlike liquid and glassy $GeSe_2$ for which we have seen that homopolar bonds and miscoordinations are an important structural feature. The occurrence of layered regions, at the very heart of the *layers* conjecture, is based on the evaluation of the **k**-vector dependent structure factor $A(\mathbf{k})$ and its spherical average $S(k)$:

$$S(k) = \frac{1}{N_k} \sum_{|\mathbf{k}|=k} A(\mathbf{k}), \tag{6.1}$$

where N_k are the N vectors $\mathbf{k}$ for which $|\mathbf{k}| = k$, the available $\mathbf{k}$ vectors being discretized. Deviations from the average $S(k)$ are given by the second moment:

$$M^{(2)}(k) = \frac{1}{N_k} \sum_{|\mathbf{k}|=k} [\langle A(\mathbf{k})^2 \rangle - \langle S(k) \rangle^2] / \langle S(k) \rangle^2, \tag{6.2}$$

where $\langle\rangle$ means an equilibrium average. A value of 1 for $M^{(2)}(k)$ corresponds to Gaussian statistics [27], while larger $M^{(2)}(k)$ indicate the formation of planes.

In the *cluster–voids* approach, a prepeak is found in the Bhatia–Thornton concentration–concentration partial structure factor $S_{CC}(k)$ [10] for a system made of 'clusters' and 'voids' particles [18, 21]. While we took Si or Ge to define the coordinates of the clusters, the voids are determined via a Voronoi analysis [29, 30], with the vertices of the Voronoi polyhedra as positions of the void particles. From the positions of clusters (M = Si, Ge) and voids (V) the partial structure factors $S_{VV}(k)$, $S_{VM}(k)$, and $S_{MM}(k)$ are derived, with the corresponding Bhatia–Thornton $S_{CC}(k)$ taking the form

$$S_{CC}(k) = c_V\, c_M\, [c_M\, S_{VV}(k) + c_V\, S_{MM}(k) - 2(c_V c_M)^{1/2}\, S_{VM}(k)], \tag{6.3}$$

where c_M is the concentration of cluster particles and c_V the concentration of voids.

The results shown in figures 6.9 and 6.10 for liquid SiO_2 and liquid $GeSe_2$, reveal that $M^{(2)}(k)$ is smaller than 1 for any k, this means that crystalline-like layers are absent in our systems. Therefore, we have obtained a clear indication that the appearance of a FSDP does not correspond to the existence of layers. By turning to the *cluster–voids* approach, it turns out that for both liquids, the Bhatia–Thornton $S_{CC}(k)$ calculated on the system made of clusters and voids is characterized by a peak at the location of the FSDP in the total structure factor (figures 6.9 and 6.10). Therefore, at a first sight, one could conclude that the cluster–void scheme is validated by the behavior of liquid SiO_2 and liquid $GeSe_2$, in line with early indications collected for vitreous silica [21]. However, before concluding on the general validity of this model, one has to check whether or not the peak is also present when the FSDP is absent. To work on this issue, we resorted to the LDA model for liquid $GeSe_2$ referred to in section 3.6.5 since in this case the FSDP in the total structure factor is absent. As it can be seen in figure 6.11, both $M^{(2)}(k)$ and $S_{CC}(k)$ are close to those obtained for the GGA model of liquid $GeSe_2$ in figure 6.10, that is to say the one featuring a FSDP in the total structure factor. In particular, the observation of a peak at the FSDP location in $S_{CC}(k)$ obtained within the 'cluster–voids' hypothesis [21] reveals this criterion cannot be associated with the occurrence of a FSDP in the total structure factor since the peak is there even when the FSDP does not manifest itself in the total structure factor.

In summary, we were able to demonstrate that the FSDP is not correlated to crystalline-like layers, while cluster–void correlations are common to all disordered networks examined, regardless of their featuring or not a FSDP in the total structure factor. Despite the interest of the conjectures advanced to account for the FSDP, one can conclude that the only criterion standing up to criticism with regard to its

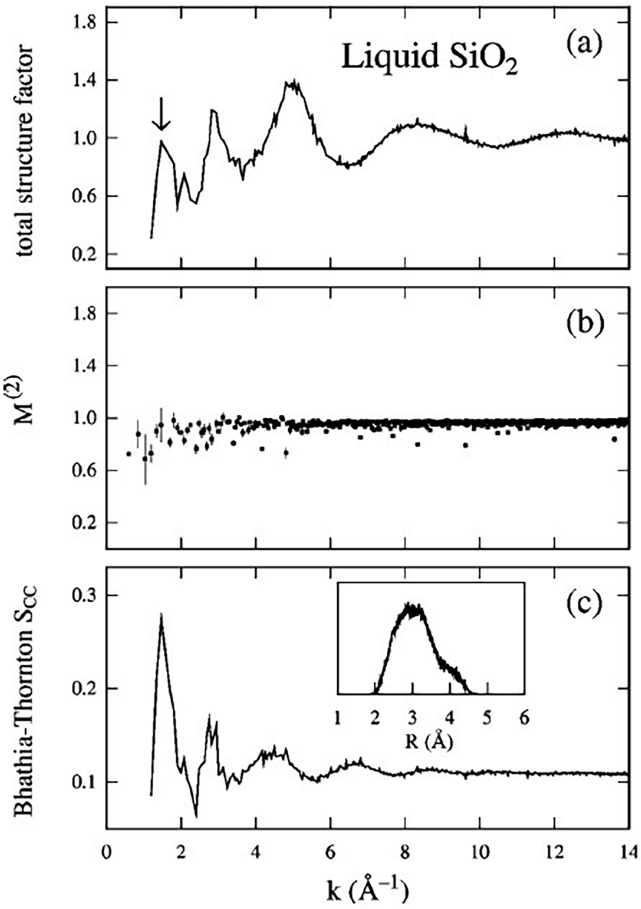

Figure 6.9. An analysis of the atomic configurations of liquid SiO_2 obtained by first-principles molecular dynamics at $T = 3500$ K [28, 31]. (A) Neutron total structure factor; (B) second moment $M^{(2)}(k)$ (see equation (6.2)); (C) Bhatia–Thornton $S_{CC}(k)$ for the cluster–void system (see equation (6.3)). The inset shows the distribution of radii corresponding to the void particles. The arrow indicates the position of the first-sharp diffraction peak. Reprinted figure with permission from [49]. Copyright (2001) by AIP Publishing.

general validity is the one linking the FSDP to the presence of a predominant structural unit, as detailed at the beginning of section 6.3.1. There we had invoked the comparative study carried out at two different temperatures for liquid $GeSe_2$ [16] to point out the different structural properties and the different intensities of the FSDP found as a function of the temperature.

6.3.2 FSDP in the concentration–concentration partial structure factor

We have seen that the establishment of a correlation between the presence of the FSDP and structural features at the atomic scale can be obtained by invoking a predominant motif, as the tetrahedron for Ge_xSe_{1-x} systems. This motif is indeed

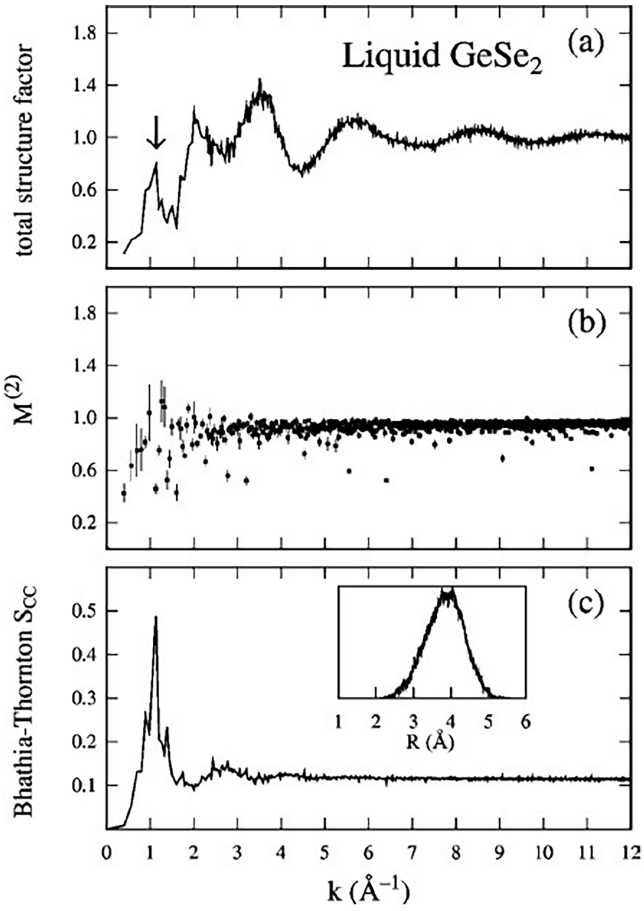

Figure 6.10. The same as in figure 6.9, but for liquid $GeSe_2$ at $T = 1050$ K [32]. Reprinted figure with permission from [49]. Copyright (2001) by AIP Publishing.

discernible in disordered network-forming systems and can even be recovered in simple models of charge hard spheres [4]. For the sake of clarity, let us call $FSDP_{tot}$ the FSDP in the total (neutron) structure factor we have considered so far. More subtle is to rationalize the existence of the FSDP in the partial structure factors and, in particular, in the concentration–concentration structure factor $S_{CC}(k)$, a very elusive feature since related to fluctuations of concentration on intermediate range order scales. We shall term hereafter this feature $FSDP_{cc}$. To begin our search of a microscopic (atomic) origin of $FSDP_{cc}$, we can refer to the behavior of the FSDP height (FSDP-*h* in the following) in liquid $GeSe_2$ (section 6.2.2 and [7]). FSDP-*h* was found highly dependent on time, as proved by the associated error bars (20%). This observation prompted us to reanalyze the trajectories of liquid $GeSe_2$ by considering the changes in time of the height of $FSDP_{cc}$, that takes values in between a minimum of 0.04 and a maximum of 0.36. We have separated the trajectories in two different subsets, depending on the values of the height of $FSDP_{cc}$ that can be higher or

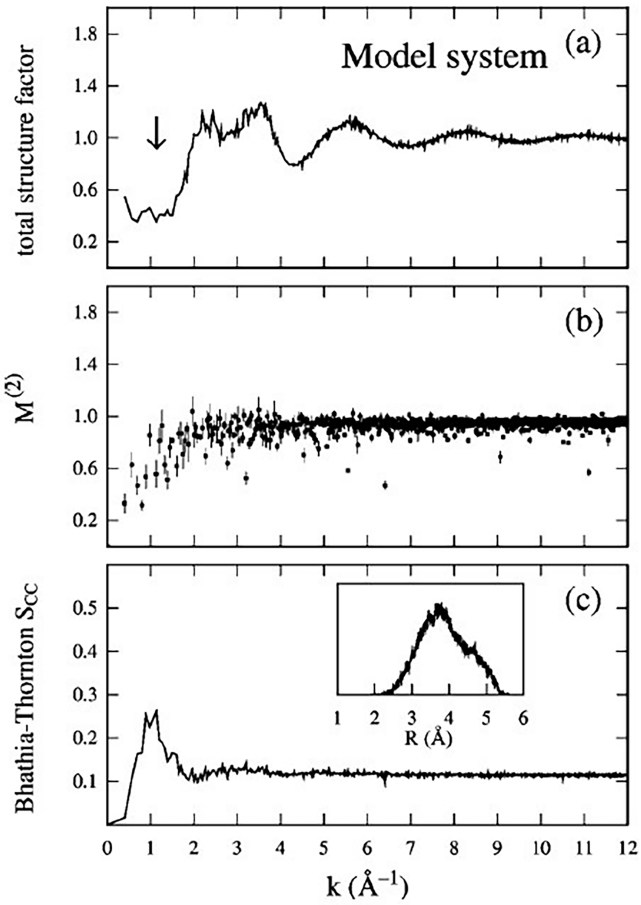

Figure 6.11. The same as in figure 6.10, but for a model of liquid $GeSe_2$ which does not show a FSDP in the total structure factor (see figure 3.6 and references therein). The arrow indicates the position of the first-sharp diffraction peak for liquid $GeSe_2$ at $T = 1050$ K (see figure 6.10). Reprinted figure with permission from [49]. Copyright (2001) by AIP Publishing.

smaller than the average 0.136. These two subsets are referred to as $\mathcal{E}_{low}$ (FSDP-h in $S_{CC}(k) \leqslant 0.136$) and $\mathcal{E}_{high}$ (FSDP-h in $S_{CC}(k) > 0.136$).

By taking advantage of this definition we introduce a new strategy for the identification of structural features that correspond to vanishing or sizeable values for the intensity of $FSDP_{cc}$ [33]. As a first indication (see figure 6.13), we can notice that $S_{GeGe}(k)$ averaged over $\mathcal{E}_{high}$ is in much better agreement with experiments than its counterpart calculated on the full trajectory and than the same property calculated over $\mathcal{E}_{low}$.

This improvement is also found in S_{CC} and $S_{NC}(k)$, which are in better agreement with experiments when calculated by considering the trajectory $\mathcal{E}_{high}$ (figure 6.14). Therefore, it appears that our search of a correlation between the height of $FSDP_{cc}$ and specific structural feature is fully legitimate and can bring new information on

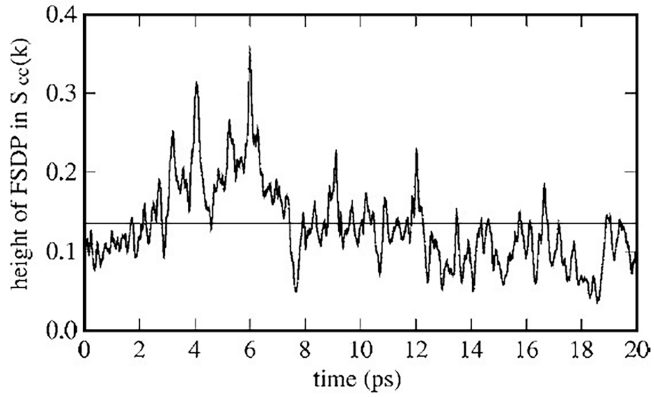

Figure 6.12. Time evolution of the height of the FSDP in $S_{CC}(k)$ for liquid $GeSe_2$. The average value of 0.136 is indicated by a horizontal line and is used to distinguish between the two sets of instantaneous configurations $\mathcal{E}_{low}$ and $\mathcal{E}_{high}$. Reprinted figure with permission from [33]. Copyright (2007) by the American Physical Society.

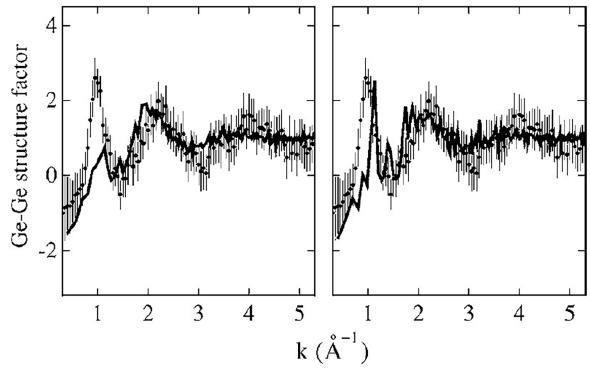

Figure 6.13. Ge–Ge partial structure factor for liquid $GeSe_2$. Experiment: dots with error bars [6] compared to the FPMD result obtained by averaging separately over all configurations in $\mathcal{E}_{low}$ (left) and $\mathcal{E}_{high}$ (right). Reprinted figure with permission from [33]. Copyright (2007) by the American Physical Society.

the atomic-scale origins of $FSDP_{cc}$. The idea is to perform the analyses employed for the studies of liquid and glassy $GeSe_2$ but on the two separate trajectories. Since we obtained close values for the coordination numbers, the bond-angle distributions, the pair correlation functions and the ring statistics on these two trajectories, we focused our attention on the number of Ge atoms belonging to two, one and zero fourfold rings (termed Ge(n) with $n = 2$, 1, and 0, respectively (see figure 6.15)).

The tetrahedra having in common only one Se atom are those contributing to the case $n = 0$, while those sharing two Se atoms ($n = 1$, 2) are those corresponding to edge-sharing connections. We found that the only notable difference between $\mathcal{E}_{low}$ and $\mathcal{E}_{high}$ in this respect is the larger value of Ge(2) in $\mathcal{E}_{high}$ (11% for $\mathcal{E}_{high}$ and 7.5% for $\mathcal{E}_{low}$) of the total number of Ge atoms. A typical configuration having a Ge(2) atom is made of two fourfold rings in a chain fashion and sharing a Ge(2) atom only. An example is given in figure 6.15 where one can observe a Ge(1)–Ge(2)–Ge(1) chain.

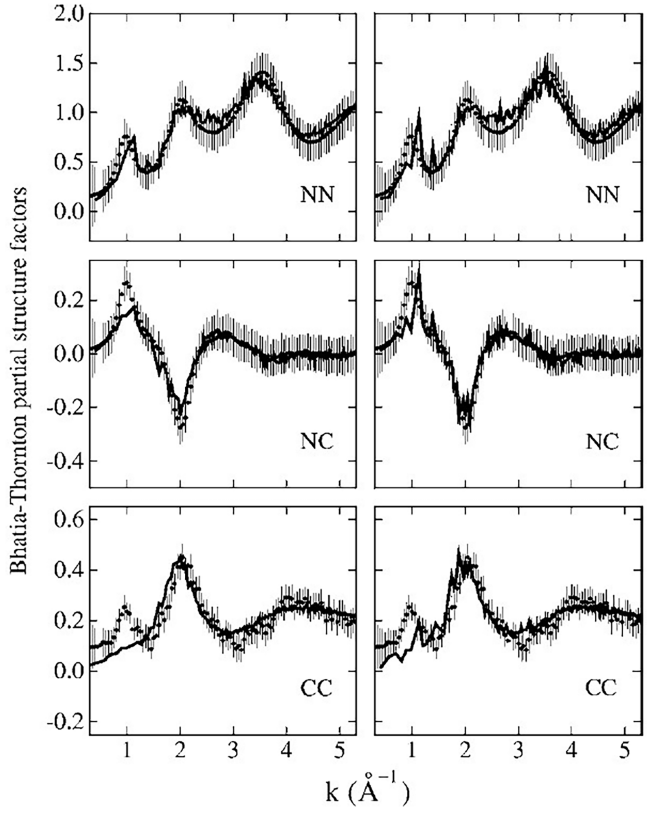

Figure 6.14. The same as in figure 6.13, but for the Bhatia–Thornton structure factors. Reprinted figure with permission from [33]. Copyright (2007) by the American Physical Society.

We found useful to select these configuration and name them Ge*. Interestingly, the number of Ge* in $\mathcal{E}_{\text{high}}$ is higher than in $\mathcal{E}_{\text{low}}$ (8.5% vs 7.5%, respectively).

It is important to realize that not all Ge(2) atoms form Ge* subunits[2], since some of them share not only a Ge(2) atom but in addition a Se atom threefold coordinated. This is exemplified in figure 6.15 where we have highlighted the difference between a Ge(2) atom [Ge(2)^{a}] being part of a Ge* unit and another Ge(2) atom [Ge(2)^{b}], corresponding to a configuration that features also a connection to a Se atom. In other words, ring 2 and ring 3 do not form a Ge* unit as opposed to ring 1 and ring 2. This classification allows pushing further the search of correlations between the height of FSDP_{cc} and the number of Ge(2) atoms and, in particular, of Ge* units.

To this end, we have recorded for each instantaneous configuration the height of FSDP_{cc} by obtaining its average value and error bar, to be linked to the different values of Ge(n) that are also extracted from the same configurations. No correlation is found between the amount of Ge(n) ($n = 0,1$) and the FSDP-h in the partial structure factor $S_{\text{GeGe}}(k)$. Similarly, no correlation with FSDP-h is found for $S_{\text{GeSe}}(k)$ and

[2] Ge* are defined in this section both as 'units' or 'subunits'.

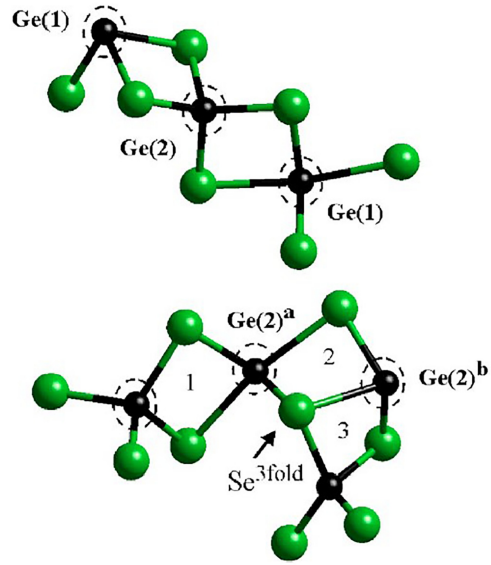

Figure 6.15. Snapshots of structural subunits found in our model of liquid $GeSe_2$. Ge atoms are black and Se atoms are green. Bonds are drawn when two atoms are separated by less than 3 Å, the first minimum in the Ge–Se pair correlation function. Ge atoms forming a Ge* subunit are surrounded by a dashed line. Reprinted figure with permission from [33]. Copyright (2007) by the American Physical Society.

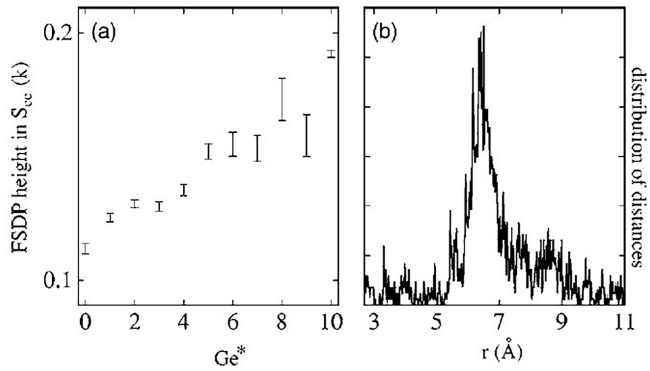

Figure 6.16. Left: height of the FSDP in $S_{CC}(k)$ as a function of the number of Ge* subunits. Right: distribution of distances between pairs of Ge atoms at the opposite ends of Ge* subunits. Reprinted figure with permission from [33]. Copyright (2007) by the American Physical Society.

$S_{SeSe}(k)$ for all values of n, this result being due to their little sensitivity to the different kind of trajectories, namely $\mathcal{E}_{low}$ or $\mathcal{E}_{high}$. While the height of the FSDP in $S_{GeGe}(k)$ is not sensitive to the occurrence of Ge(0) or Ge(1), a linear growth is observed as a function of the number of Ge* units, the height of FSDP $_{cc}$ increasing with the number of Ge*, as shown in figure 6.16(a). *Accordingly, we are in a position to label Ge* as the main structural motif accounting for the existence of the FSDP in $S_{CC}(k)$, thereby providing a clear link between the occurrence of fluctuations of concentration on*

intermediate range scales and the presence of Ge(1)–Ge(2)–Ge(1) chains. As a final step of this analysis, it is important to find out whether there are distances related to the Ge* units that can be taken as corresponding to intermediate range order. This is substantiated by the frequency of occurrence of distances between pairs of Ge atoms at the ends of the chain in the Ge* units (figure 6.16(b)). The peak noticeable at ~6.5 Å in figure 6.16(b) is consistent with the relationship between the value of r in real space (for a given peak) and the value of k of a corresponding peak in reciprocal space, $k \cdot r \approx 7.7$. We have obtained this relationship by accounting for the first maximum of the spherical Bessel function and by knowing that the FSDP position for liquid $GeSe_2$ is at 1.13 $Å^{-1}$. These results provide a prototypical example of the possibilities offered by molecular dynamics (and, in particular, by FPMD as a method to describe realistically chemical bonding at finite temperatures) to establish a correspondence between a measurable quantity and a specific structural detail. Each instantaneous configurations contains a lot of precious information that are quite often overlooked or not sufficiently exploited since one has as primary goal the calculation of average properties. In this case, little would have been learned by limiting our analysis to taking averages on the whole trajectory. On the contrary, by taking advantage of the mere observation that the FSDP strongly fluctuates in time, we were able to derive a methodology that highlights two contrasting behaviors, related to different amounts of Ge(1)–Ge(2)–Ge(1) chains of connected Ge atoms.These are at the very origin of the FSDP in the concentration–concentration structure factor $S_{CC}(k)$.

6.4 FSDP in disordered network: some considerations before to go on

So far we have seen that glassy (and liquid) $GeSe_2$ have an intriguing behavior in terms of partial and total structure factors, driving many questions on the nature of intermediate range order that go beyond the simple interest for a given system. The relevant pieces of evidence can be summarized as follows:

1. The presence of the FSDP in the total structure factor can be associated to a predominant structural motif. While this simple statement does not undermine all models developed in the search of an alternative origin, we can safely assume that such a simple explanation has a general validity, substantiated by MD approaches of an increasing complexity (from charges hard spheres to first-principles calculations).
2. While the FPMD approach based on the PW-GGA scheme is able to provide an excellent agreement between theory and experiment for the total neutron structure factor, there is striking disagreement at the level of the partial structure factors, in particular for $S_{GeGe}(k)$ and the concentration–concentration partial structure factor $S_{CC}(k)$. The presence of the FSDP in this latter, clearly visible in experiments, and meaning fluctuations of concentration on intermediate range distances, is not confirmed by our level of theory, since the FSDP in $S_{CC}(k)$ is simply absent in the liquid and is barely discernible in the glass.
3. The situation becomes quite paradoxical if one considers that the absence of the FSDP in the early models of disordered $GeSe_2$ was proposed as a general feature of AX_2 networks. On a purely intuitive basis, this cannot be taken as

a demonstration that models not accounting explicitly for the electronic structure are as performing as FPMD ones, since one expects to find a difference between $S_{CC}(k)$ and $S_{zz}(k)$ for a realistic system, while they differ simply by a constant factor in a point-charged one.

4. By looking at many instantaneous configurations within a trajectory, we have realized that the FSDP in $S_{CC}(k)$ is due to specific structural units, namely the chains of edge-sharing tetrahedra. This means that the FSDP can be observed provided certain microscopic conditions are met.

The above observations call for a series of calculations to be performed in order to clarify all these issues and move ahead into a full understanding of intermediate range order in disordered network-forming materials.

1. Experiments provided evidence for the presence of the FSDP in $S_{CC}(k)$ for a set of systems. It is important to determine whether the FPMD methodology can reproduce some of these results, thereby proving that liquid $GeSe_2$ is somewhat a special case deserving unprecedented levels of accuracy in the theoretical treatment.
2. The existence of different cases differing by the presence of the FSDP in $S_{CC}(k)$ is a motivation to classify them with respect to their structural details. Are all of the systems with no FSDP in $S_{CC}(k)$ sharing the same topology? Does the absence or the presence of this feature have an impact on (or is a consequence of) the atomic structure? Is it possible to label these networks in a comparative fashion by considering their intermediate range properties as expressed by $S_{CC}(k)$?
3. It would also be quite instructive to focus, within a first-principles scheme, on a comparison between $S_{CC}(k)$ and $S_{zz}(k)$ for some of these systems. The FSDP is absent in $S_{zz}(k)$ for a model potential of point charges. How does it behave when the electronic structure is taken into account? Is there something we can learn by considering on the same footing fluctuations of concentration ($S_{CC}(k)$) and fluctuations of charge ($S_{zz}(k)$)?

All these issues are addressed in the two sections that follow, the first in section 6.5, the second and the third in section 6.6.

6.5 Evidence of FSDP in $S_{CC}(k)$: examples

One would like to establish whether the FPMD methodology is able to capture the presence of the FSDP in the concentration–concentration for some systems. To this purpose, we have selected liquid $GeSe_4$ and liquid $SiSe_2$ [34] that were also considered in the context of our calculations on disordered network-forming materials, despite their being somewhat less representative due to the absence of experimental information on the partial structure factors[3]. These two systems were found to exhibit a higher degree of chemical order with respect to liquid and glassy $GeSe_2$, i.e. a lower number of coordinations differing from four (for Ge) and two

[3] This statement was valid at the time the calculations we are referring to were performed. Recent experimental results on the partial structure factors of glassy $GeSe_4$ can be found in [35].

(for Se) and a smaller number for homopolar bonds (this applies in particular when comparing networks of the same concentration, $GeSe_2$ and $SiSe_2$). The case of liquid $GeSe_4$ had been the object of calculations reproducing accurately the total neutron structure factor, clearly proving its character of excellent prototype of a chemically ordered network (CON) [36]. The case of liquid $SiSe_2$ was considered to ensure the availability of a model for the glassy phase [37], by concluding that the chemical order was higher than in liquid $GeSe_2$, despite the same value for the electronegativity of Ge and Si (1.8) [38]. Having invoked several times the notion of chemical order as a key tool to compare the topologies of different networks, it is instructive, before moving ahead to the explicit calculations of experimental probes relative to the structure, to have a global view of the behavior of these three disordered systems ($GeSe_4$, $SiSe_2$ and $GeSe_2$, the three in their liquid state). Table 6.3 contains data elucidating the nearest-neighbor structure of these networks, by exploiting the quantities defined in section 6.3. The same table refers also to two phenomenological models for the network structure, the random covalent network (RCN) and the CON. Both are consistent with the so-called 8−N rule, which gives the coordination number of an atom in terms of its position (column *N*) in the periodic table. The structure of a liquid at a given composition follows the RCN model if neither homopolar or heteropolar bonds are preferred. On the contrary, CON holds when the number of heteropolar bonds is the highest accessible for that composition, knowing that in any case for a given composition, the total coordination numbers for the two models are the same. With no loss of validity, we refer in this analysis to the sets of data available when the paper we refer to was published [34]. While some of these data were revisited and somewhat improved later, all of the conclusions drawn thereof remain fully valid. In particular, neither the larger systems nor alternative choices for the exchange−correlation functional changed the essence of the results.

One notices that liquid $GeSe_2$ cannot be considered as chemically ordered since n_{Se}^{Se} is far from the CON value. This same model is much more realistic that the RCN one,

Table 6.3. Values for the coordination numbers n_{Ge}, n_{Se}, n_{Si} and the total coordination number n_{tot} (also called n_{ave} in section 2.4.1) of liquids $GeSe_2$, $GeSe_4$ and $SiSe_2$. The definitions are given in section 2.4.1. Copyright (2003) courtesy IOP Publishing.

$GeSe_2$	n_{Ge}^{Ge}	n_{Ge}^{Se}	n_{Ge}	n_{Se}^{Se}	n_{Se}^{Ge}	n_{Se}	n_{tot}
FPMD	0.04	3.76	3.80	0.37	1.88	2.25	2.77
RCN	2	2	4	1	1	2	2.67
CON	0	4	4	0	2	2	2.67
$GeSe_4$	n_{Ge}^{Ge}	n_{Ge}^{Se}	n_{Ge}	n_{Se}^{Se}	n_{Se}^{Ge}	n_{Se}	n_{tot}
FPMD	0.06	3.87	3.93	1.04	0.97	2.01	2.39
RCN	1.33	2.67	4	1.33	0.67	2	2.4
CON	0	4	4	1	1	2	2.4
$SiSe_2$	n_{Si}^{Si}	n_{Si}^{Se}	n_{Si}	n_{Se}^{Se}	n_{Se}^{Si}	n_{Se}	n_{tot}
FPMD	0.02	3.90	3.92	0.13	1.95	2.08	2.69
RCN	2	2	4	1	1	2	2.67
CON	0	4	4	0	2	2	2.67

definitely unable to describe the network structure, as confirmed by the fact the coordination numbers were found to be acceptably close to experiments. Comparison with liquid $GeSe_4$ and liquid $SiSe_2$ reveals that these two systems are closer to a CON network. In particular, for liquid $GeSe_4$ this means that the majority of Ge atoms form $GeSe_4$ tetrahedra, while some of the Se atoms form homopolar bonds since the concentration is far from the stoichiometric one. Therefore, these data indicate that a transition from a network departing (moderately) from a CON (as $GeSe_2$, not featuring the FSDP in $S_{CC}(k)$) to a network more chemically ordered (as $GeSe_4$, featuring some form of FSDP in $S_{CC}(k)$, see below) occurs while increasing the content of Se atoms within the family of Ge_xSe_{1-x} disordered networks. Similarly (see below) the data on liquid $SiSe_2$ confirm the correlation between some extent of chemical order and the appearance of the FSDP in $S_{CC}(k)$.

To substantiate the previous assertions we focus on the behavior of $S_{CC}(k)$ for the systems under consideration. The case for liquid $GeSe_2$ has been already treated in section 6.2.2 and, in particular, via figure 6.2. Concerning $GeSe_4$, a new set of data were produced by starting from those published in 1998 [36][4]. As visible in figure 6.17, one obtains only a small peak in the FSDP region with the ratio between the heights of the first two peaks equal to 0.12/0.43 = 0.28, half the experimental value of 0.56. In liquid $GeSe_4$ the FSDP-like signature at 1 $Å^{-1}$ gives a ratio between the first two peaks equal to 0.45, much higher than for the $GeSe_2$ case. In the case of liquid $SiSe_2$ a distinct bump exists at the FSDP location in $S_{CC}(k)$. Despite the higher level of chemical order found in this system when compared to liquid $GeSe_2$, this is not reflected by the ratio between the intensities of the first two peaks (0.22 versus 0.28 for liquid $GeSe_2$). Nevertheless, the FSDP-like feature is clearly more discernible in the case of $SiSe_2$, by pointing out a higher amount of fluctuations of concentration than in the corresponding $GeSe_2$ network.

The above results can be commented on by invoking a correlation between the presence of the FSDP in $S_{CC}(k)$ and the amount of chemical disorder. So far, we have been able to identify two categories, the first corresponding to the absence of the FSDP in $S_{CC}(k)$ for a system (like $GeSe_2$ when modeled within FPMD at the PW-GGA level) with a sizeable deviation from chemical order while the second features a network closer to the CON model and the appearance of a discernible feature in $S_{CC}(k)$ at the FSDP location. This is also the case of the experimental results for liquid $GeSe_2$ [6]. To complete this first classification and pave the way for further studies, one needs some indication on the behavior of essentially perfect networks (no homopolar bonds and no deviations to the regular tetrahedral arrangement) as encountered in the case of amorphous GeO_2 and SiO_2, where the difference of electronegativity between the species favors ionicity. It appears that the FSDP is absent in the measured $S_{CC}(k)$ of amorphous GeO_2 [39], a result confirmed by available FPMD data on the analogous SiO_2 networks [31]. The existence of this third category of networks (perfect chemical order and no FSDP in $S_{CC}(k)$) calls for a well established classification, involving also any possible correlation existing

[4] More on liquid $GeSe_4$ and, more generally, on this specific composition can be found in chapter 8.

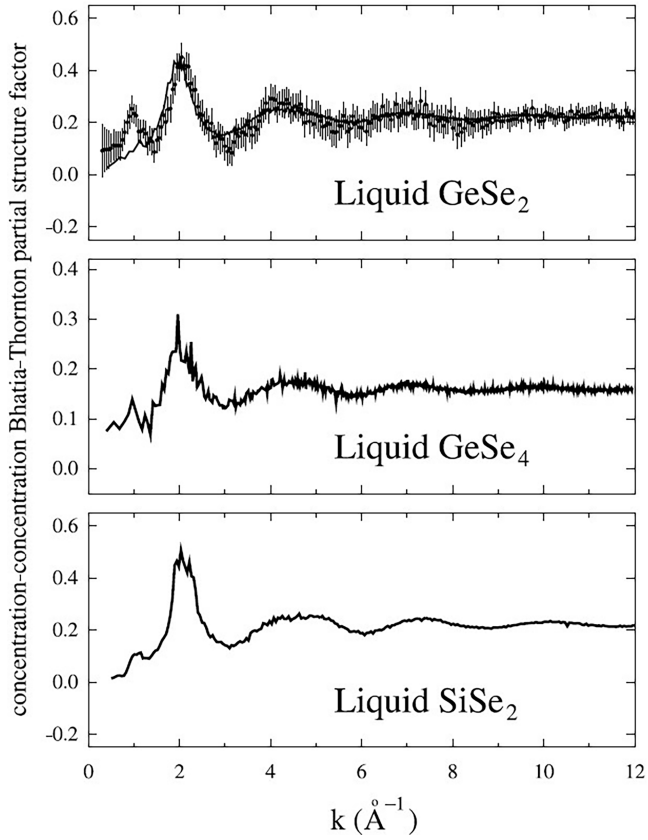

Figure 6.17. Concentration–concentration partial structure factor $S_{CC}(k)$ for liquid $GeSe_2$ [7], liquid $GeSe_4$ and liquid $SiSe_2$. The experimental data for liquid $GeSe_2$ (dots with error bars) are those of [6]. Copyright (2003) courtesy IOP Publishing.

between fluctuations of concentrations and fluctuations of charge. The idea is to establish some precise links between the atomic structures and some measurable properties, by providing information on the conditions under which the networks tend to arrange in some specific manner at the atomic scale.

6.6 What to learn from $S_{CC}(k)$ vs $S_{zz}(k)$

Before describing the behavior of $S_{CC}(k)$ and $S_{zz}(k)$ for different systems, classified according to the intensity recorded for the FSDP in $S_{CC}(k)$, it is useful to recall some definitions necessary to highlight similarities and differences among them. Let's consider a binary system made of α and β atoms in concentrations c_α and c_β and the Bhatia–Thornton concentration–concentration partial structure factor $S_{CC}(k)$ as defined via equation (2.6)

$$S_{CC}(k) = c_\alpha c_\beta \{1 + c_\alpha c_\beta \left[\left(S_{\alpha\alpha}(k) - S_{\alpha\beta}(k) \right) + \left(S_{\beta\beta}(k) - S_{\alpha\beta}(k) \right) \right] \} \tag{6.4}$$

where $S_{\alpha\alpha}(k)$, $S_{\alpha\beta}(k)$ and $S_{\alpha\beta}(k)$ are the partial structure factors defined with respect to the atomic species.

Based on both calculations and experiments, we were also able to identify three different classes of systems, introduced in the previous section. In the first class (class I) there are networks with a perfect chemical order and no FSDP in $S_{\mathrm{CC}}(k)$. For instance, we have systems like SiO_2 and GeO_2, known experimentally or by simulation [31, 39]. To the second class belong network systems with a distinct FSDP in $S_{\mathrm{CC}}(k)$, characterized by small departures from chemical order, as we have seen for of liquid $GeSe_4$ and liquid $SiSe_2$ (section 6.5). The representative structure of class III is the one we obtained via FPMD for liquid $GeSe_2$. In this case, like for class I, the FSDP is absent in $S_{\mathrm{CC}}(k)$. However, the network is far from being chemically ordered since there are a lot of structural motifs in the nearest coordination shells (section 6.2.2). In what follows, our analysis of fluctuations of concentration and fluctuations of charges on intermediate range scales is substantiated by the calculation of charge–charge structure factor $S_{zz}(k)$ for three AX_2 networks: liquid SiO_2 (class I), glassy $SiSe_2$ (class II) and liquid $GeSe_2$ (class III).

We anticipate that no FSDP shows up in any charge–charge structure factors $S_{zz}(k)$, demonstrating that no charge ordering takes place at intermediate range scales, and this regardless of the occurrence of concomitant fluctuations of concentration.

6.6.1 Calculating $S_{zz}(k)$

To obtain $S_{zz}(k)$ in the DFT–FPMD framework, one has to consider the valence electron density built in the total charge density made of ionic and electronic parts, $\rho_{\mathrm{t}}(\mathbf{r}) = \sum_i z_i \delta(\mathbf{r} - \mathbf{r}_i) + \rho_{\mathrm{e}}(\mathbf{r})$:

$$S_{zz}(k) = N^{-1}\langle z_{\mathrm{v}}^2\rangle^{-1} \int d\mathbf{r} d\mathbf{r}' \rho_{\mathrm{t}}(\mathbf{r})\rho_{\mathrm{t}}(\mathbf{r}')\mathrm{e}^{i\mathbf{k}\cdot(\mathbf{r}-\mathbf{r}')}. \tag{6.5}$$

Since in the pseudopotential approach the valence electrons are the only ones accounted for in $\rho_{\mathrm{e}}(\mathbf{r})$, the ionic charges z_i are $z_A = +4$ and $z_X = +6$ for the case of the systems treated hereafter. In equation (6.5) we assume the spherical average over the orientations of $\mathbf{k}$, where N is the number of atoms and $\langle z_{\mathrm{v}}^2\rangle$ is a normalization factor, $\langle z_{\mathrm{v}}^2\rangle = z_{\mathrm{v}A}^2 c_A + z_{\mathrm{v}X}^2 c_X$. In the equation for $\langle z_{\mathrm{v}}^2\rangle$, $z_{\mathrm{v}A} = +4$ and $z_{\mathrm{v}X} = -2$ are the charges assigned to A and X atoms when a pointlike charge model (PLC) is selected. In the limit $k \to \infty$, $S_{zz}(\infty) = \langle z^2\rangle/\langle z_{\mathrm{v}}^2\rangle$, with $\langle z^2\rangle = z_A^2 c_A + z_X^2 c_X$. For AX_2 systems this gives $S_{zz}(\infty) = 3.66$.

When the PLC model holds, the total charge density takes the form $\rho_{\mathrm{t}}(\mathbf{r}) = \sum_i z_{\mathrm{v}i}\delta(\mathbf{r} - \mathbf{r}_i)$. The charge–charge structure factor $S_{zz}(k)$ becomes proportional to $S_{\mathrm{CC}}(k)$:

$$\begin{aligned} S_{zz}^{\mathrm{PLC}}(k) &= N^{-1}\langle z_{\mathrm{v}}^2\rangle^{-1} \sum_{ij} z_{\mathrm{v}i} z_{\mathrm{v}j} e^{i\mathbf{k}\cdot(\mathbf{r}_i - \mathbf{r}_j)} \\ &= (c_{\mathrm{A}} c_{\mathrm{X}})^{-1} S_{\mathrm{CC}}(k). \end{aligned} \tag{6.6}$$

6.6.2 Comparing $S_{zz}(k)$ and $S_{CC}(k)$ for the three classes of networks

As a first example, we consider a system of class I, liquid SiO_2, for which we have reproduced and extended FPMD simulations published in [28, 31]. In this system, prototype of 'perfect' chemical order, the Si atoms are linked within tetrahedra to O atoms via corner-sharing connections. In figure 6.18, the structure factors $S_{zz}(k)$ and $S_{CC}(k)$ for liquid SiO_2 are compared, providing evidence that $S_{zz}(k)$ is very much different from the concentration–concentration structure factor for which we employ the definition of equation (6.6), that is $S_{CC}(k) \sim S_{zz}^{PLC}(k)$.

Also, the absence of the FSDP in $S_{zz}(k)$ (small signatures in the FSDP region not being statistically significant) are indicative of no charge fluctuations on IRO scales. It is of interest to observe that this system might be conjectured as the best candidate to be described by a pointlike charge model, due to the high ionicity of the bonds between Si and O atoms. However, this is not the case since there are noticeable differences between $S_{CC}(k)$ and $S_{zz}(k)$, illustrating the fact that structural order and

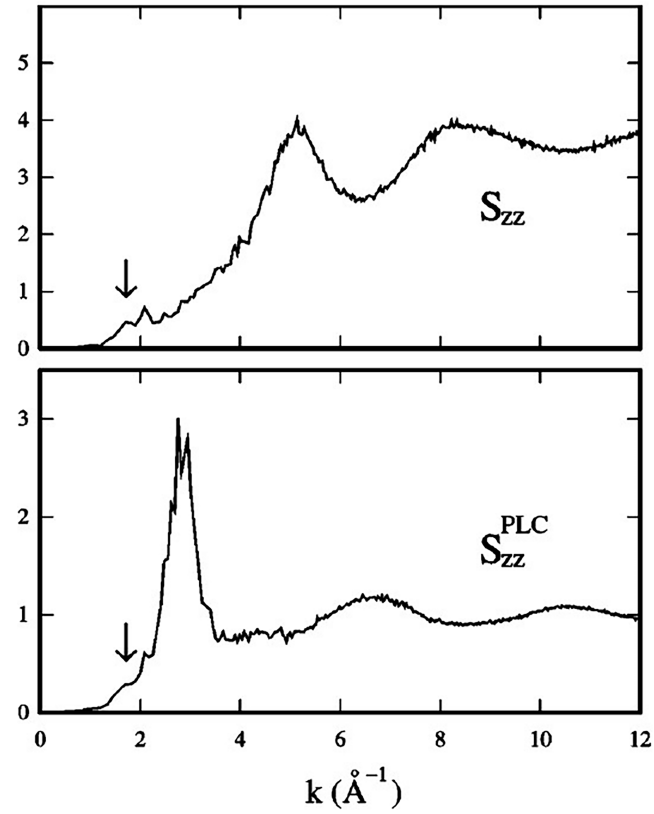

Figure 6.18. Upper panel: charge–charge structure factor $S_{zz}(k)$ of liquid SiO_2 at $T = 3500$ K. Lower panel: $S_{CC}(k)$ of liquid SiO_2 at $T = 3500$ K. $S_{CC}(k)$ is normalized as in equation (6.6). The arrows indicate the location of the FSDP in the total neutron structure factor. Reprinted figure with permission from [42]. Copyright (2004) by the American Physical Society.

charge order express two different physical properties, as a consequence of the delocalized and spatially distributed nature of the electron charge.

As a second example, turning to class II, we consider amorphous $SiSe_2$ that is characterized, as its liquid counterpart, by substantial chemical order and a few structural defects. FPMD helped to show that its atomic structure is made of both corner-sharing and (predominantly) edge-sharing connections [37] with only a few homopolar bonds [37, 40, 41], in a way consistent with coordination numbers typical of a CON-like structure, $n_{Si} = 3.95$, $n_{Se} = 2.04$, $n_{Si}^{CON} = 4$, $n_{Se}^{CON} = 2$. In figure 6.19 a peak is visible at the FSDP location in $S_{zz}^{PLC}(k)$, to be attributed mostly to Si–Si correlations. However, as for the class I system seen before, the charge–charge structure factor $S_{zz}(k)$ does not show any FSDP peak or any signature at the FSDP location (figure 6.19). Remarkably, $S_{zz}(k)$ features a bump at the main peak k value in $S_{zz}^{PLC}(k)$, $k_M \sim 2$ Å^{-1}, to indicate that both fluctuations of charge and fluctuations of concentration are present at short range. However, the peak at $k_{FSDP} = 1$ Å^{-1} proves that fluctuations of concentration are still noticeable for larger distances. We

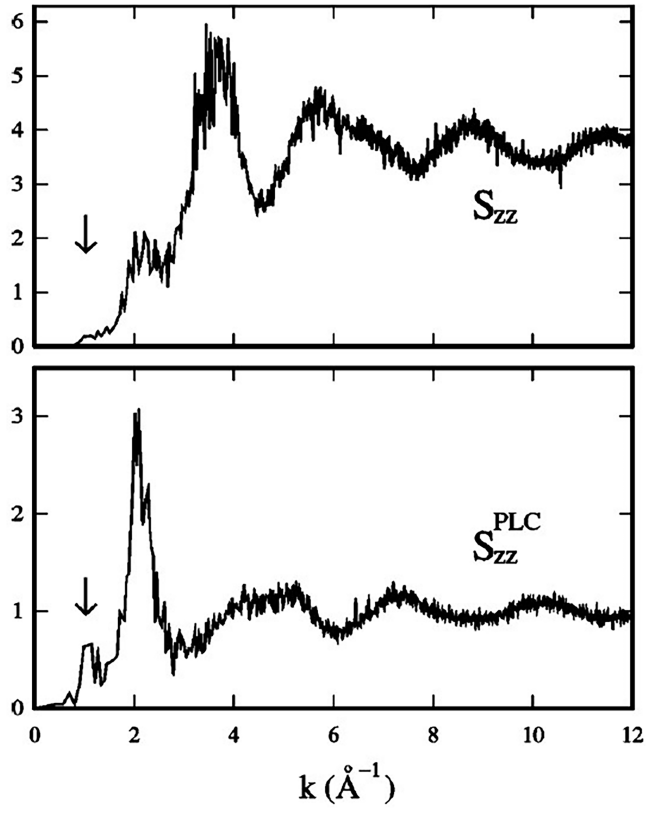

Figure 6.19. Upper panel: charge–charge structure factor $S_{zz}(k)$ of amorphous $SiSe_2$ at $T = 300$ K. Lower panel: $S_{CC}(k)$ of amorphous $SiSe_2$ at $T = 300$ K. $S_{CC}(k)$ is normalized as in equation (6.6). The arrows indicate the location of the FSDP in the total neutron structure factor. Reprinted figure with permission from [42]. Copyright (2004) by the American Physical Society.

concluded that in glassy $SiSe_2$ fluctuations of concentration over IRO length scales are correlated to a small deviation from chemical order, leading to the appearance of a FSDP in the $S_{CC}(k)$, otherwise absent in a network belonging to class I.

As we have mentioned before, to class II belongs also liquid $GeSe_2$ as measured using the method of isotopic substitution in neutron diffraction [6] since a FSDP characterizes $S_{CC}(k)$, as due to correlations involving mostly Ge–Ge interactions. On the other hand, as already underlined in section 6.2.2, the FSDP is absent in $S_{CC}(k)$ as calculated by FPMD, indicating that the absence of this feature can have two distinct origins, the first being the establishment of perfect chemical order (class I) or a high level of structural disorder (as in liquid $GeSe_2$ via FPMD class III). The charge–charge structure factor $S_{zz}(k)$ of such class III system behaves similarly to the case of glassy $SiSe_2$ (see figure 6.20). *Therefore, the lack of any feature at the FSDP location confirms that no charge ordering occurs at IRO scales in disordered network-forming materials. This conclusion holds regardless of the presence of fluctuations of concentration on the same length scale.*

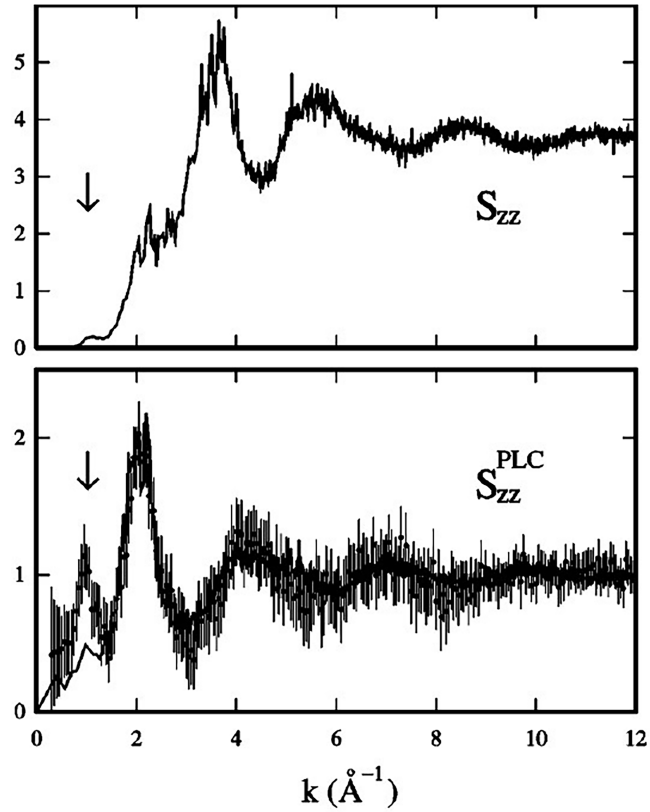

Figure 6.20. Upper panel: charge–charge structure factor $S_{zz}(k)$ of liquid $GeSe_2$ at $T = 1050$ K. Lower panel: $S_{CC}(k)$ of liquid $GeSe_2$ at $T = 1050$ K. $S_{CC}(k)$ is normalized as in equation (6.6). Full line: FPMD [42], dots with error bars: experimental results [6]. The arrows indicate the location of the FSDP in the total neutron structure factor. Reprinted figure with permission from [42]. Copyright (2004) by the American Physical Society.

To summarize and rationalize the results presented here, one can postulate that the appearance of fluctuations of concentration on IRO distances is due the constraint of charge neutrality. For a perfect network, no local variations of the average concentration are required since all atoms of the same species have the same valence. As a result, no FSDP exists in the concentration–concentration structure factor $S_{CC}(k)$. The situation is different when there is a non-negligible amount of chemical disorder via the occurrence of different valence states. In order to have charge neutrality over intermediate distances, the existence of valence states of different nature has to correspond to local variations in the network. This has the effect of producing deviations in the local concentration from the average value, giving rise to fluctuations of concentration at intermediate range distances and to the appearance of a FSDP in $S_{CC}(k)$.

6.7 Improving the description of chemical bonding

6.7.1 Contours of the GGA issue for chalcogenides

The previous sections of this chapter have focused on results for disordered chalcogenides obtained within the FPMD methodology. We have stressed the importance of going beyond the LDA approximation by using GGA schemes, as discussed and exemplified in section 3.6.5 and in section 4.2.1. The GGA scheme selected over our first period of involvement with FPMD simulations of chalcogenides (1995–2008 if taken from the very start) is the one devised by Perdew and Wang [43, 44]. In this section, we shall rationalize our choice of seeking and using alternative GGA recipes with the intention of improving the comparison with experiments for the structural properties of our prototype networks, namely liquid and glassy $GeSe_2$. We recall that the PW choice led to a very satisfactory agreement with experiments for the total neutron structure factor over the entire range of k values as shown in section 6.2.2. This was due to an improved account of the *ionic character of bonding*, as shown in section 3.6.5. However, the careful comparison of each partial pair correlation function showed, especially in the Ge–Ge case, the existence of a residual disagreement between our calculations and the experimental counterpart. The previous section has underscored as the most elusive aspect of this disagreement the one concerning the first-sharp diffraction peak in the concentration–concentration structure factor. In which direction do we have to search when looking for improvements?

6.7.2 Why BLYP?

A first observation concerns the shape of the Ge–Ge correlation function, the experimental counterpart being more structured (figure 6.3). Also the Ge–Ge distances are 15% longer than the measured values (table 6.1). These features can be ascribed, at least tentatively, to an overestimate of the metallic character of bonding. Therefore, when choosing an alternative GGA scheme, it would be desirable to select a scheme capable of optimizing the distribution of the valence-charge densities along the bonds. This means we are interested in GGA functionals promoting a more localized distribution of the valence electrons, delocalization

effects being typical of schemes reminiscent of the uniform electron-gas model, as the PW one. Within this context, this section reconsiders liquid and glassy $GeSe_2$ as obtained by using a GGA scheme based on the so-called BLYP XC functional [45, 46] (B stands for the exchange energy [45] by Becke, and LYP by the correlation energy by Lee, Yang and Parr [46]). For the correlation energy, BLYP does not contain any assumption on its uniform electron-gas character, motivating its selection as an appropriate XC functional to perform better than the PW scheme. Indeed, this scheme is expected to increase the localized behavior of the electron density by lowering electronic delocalization that favors the metallic character. BLYP is thought to perform better than PW when the difference of electronegativity between the components Δ_{el} is moderate. In the opposite case (large Δ_{el}) the ionic contribution is large enough to promote charge transfer regardless of the specific XC functional, as it occurs for disordered SiO_2 ($\Delta_{el} = 1.54$), for which LDA proved fairly adequate, at least for structural properties. When one lowers Δ_{el}, the valence-charge density along the bonds is more important and, as a consequence, the relative weight of the covalent and ionic character is harder to appreciate. We have already encountered this case with the behavior of liquid $GeSe_2$, for which $\Delta_{el} = 0.54$. The choice of BLYP corresponds to the attempt of minimizing electronic delocalization effects that are unavoidable and yet undesirable when there is a competition between ionic and covalent contributions. It should be kept in mind, however, that the use of BLYP or of any other GGA recipe favoring electronic localization cannot be based on the simple analysis of the Δ_{el} value. Other factors should be included, such as the bonding changes with thermodynamic parameters as pressure and temperature. There is a direct and unambiguous way of checking whether the use of BLYP can lower the metallic character of bonding: the calculation of the electronic density of states. As shown in figure 6.21, at $T = 1050$ K the electronic densities of states calculated via the BLYP approach is characterized, around the Fermi level, by a deeper pseudogap when compared to the PW one.

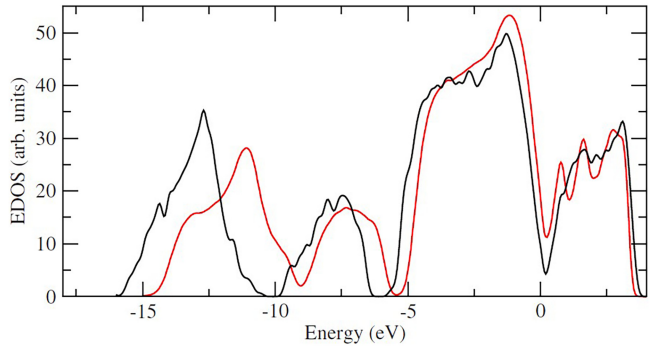

Figure 6.21. Electronic density of states (Kohn–Sham eigenvalues) of liquid $GeSe_2$: black line: BLYP results [47], red line: PW results [7]. A Gaussian broadening of 0.1 eV has been employed. Reprinted figure with permission from [47]. Copyright (2009) by the American Physical Society.

6.7.3 Liquid $GeSe_2$: BLYP vs PW, direct space and short-range properties

The analysis of the partial pair-correlation functions $g_{\alpha\beta}^{\mathrm{exp}}(r)$, $g_{\alpha\beta}^{\mathrm{PW}}(r)$ and $g_{\alpha\beta}^{\mathrm{BLYP}}(r)$ (figure 6.22) is an essential tool to understand whether or not the BLYP recipe brings substantial changes in the structure with respect to PW and at which (short or intermediate) range. Hints can be obtained by looking first at the numbers of neighbors and peak positions given in tables 6.4 and 6.5. Se–Se correlations obtained with the BLYP scheme are very close to those obtained when using PW, as indicated by the values for the first-coordination shells in table 6.4 and by visual inspection of $g_{\mathrm{SeSe}}^{\mathrm{BLYP}}(r)$ and $g_{\mathrm{SeSe}}^{\mathrm{PW}}(r)$ (figure 6.22). This is a typical feature of all calculations performed on chalcogenides with the intent of comparing among different XC functionals, the various approaches having little impact on the Se environment, not too dissimilar in terms of structural features to experiments. The behavior of Ge–Ge correlations is drastically different. The BLYP scheme performs better than the PW one by producing a clear first maximum in $g_{\mathrm{GeGe}}^{\mathrm{BLYP}}(r)$ due to homopolar Ge–Ge bonds, and a pronounced first minimum, thereby better

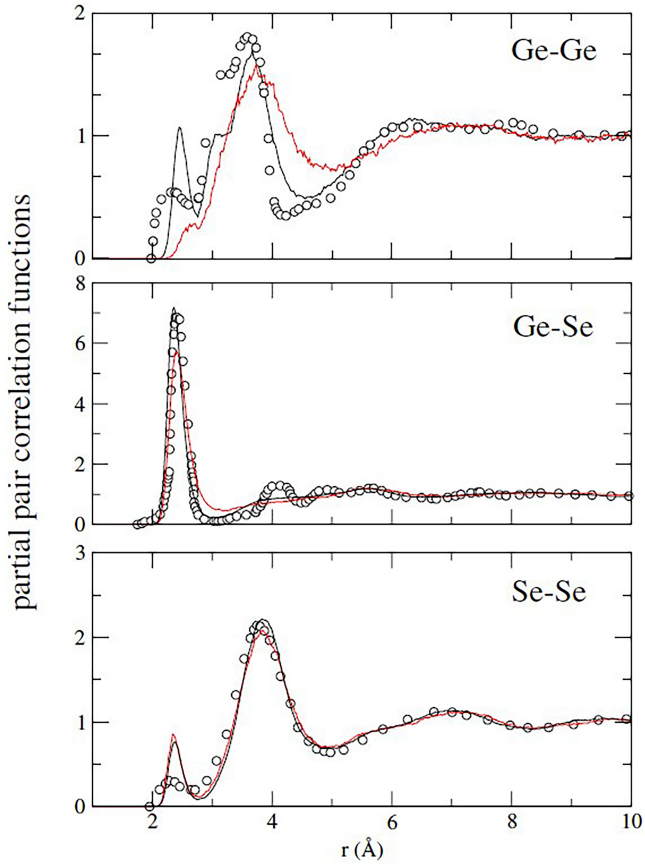

Figure 6.22. Partial pair-correlation functions for liquid $GeSe_2$: black line: BLYP results [47], red line: PW results [7], open circles: experimental results [6]. Reprinted figure with permission from [47]. Copyright (2009) by the American Physical Society.

Table 6.4. First peak position FPP and second peak position SPP in experimental [6] and calculated pair correlation functions within the PW and BLYP exchange–correlation functional. The integration ranges for the coordination numbers n_α^β and m_α^β are 0-2.6 Å, 2.6-4.2 Å for $g_{GeGe}^{exp}(r)$, 0-3.1 Å, 3.1-4.5 Å for $g_{GeSe}^{exp}(r)$ and 0-2.7 Å, 2.7-4.8 Å for $g_{SeSe}^{exp}(r)$. Error bars are the standard deviations from the mean for subaverages of 2 ps. Reprinted table with permission from [47]. Copyright (2009) by the American Physical Society.

$g_{\alpha\beta}(r)$	FPP (Å)	n_α^β	SPP (Å)	m_α^β
$g_{GeGe}^{exp}(r)$	2.33 ± 0.03	0.25 ± 0.10	3.59 ± 0.02	2.9 ± 0.3
$g_{GeGe}^{BLYP}(r)$	2.45 ± 0.10	0.22 ± 0.01	3.67 ± 0.10	2.70 ± 0.06
$g_{GeGe}^{PW}(r)$	2.70 ± 0.10	0.04 ± 0.01	3.74 ± 0.05	2.74 ± 0.06
$g_{SeSe}^{exp}(r)$	2.30 ± 0.02	0.23 ± 0.05	3.75 ± 0.02	9.6 ± 0.3
$g_{SeSe}^{BLYP}(r)$	2.38 ± 0.02	0.33 ± 0.01	3.83 ± 0.02	8.9 ± 0.6
$g_{SeSe}^{PW}(r)$	2.34 ± 0.02	0.37 ± 0.01	3.84 ± 0.02	9.28 ± 0.04
$g_{GeSe}^{exp}(r)$	2.42 ± 0.02	3.5 ± 0.2	4.15 ± 0.02	2.9 ± 0.3
$g_{GeSe}^{BLYP}(r)$	2.36 ± 0.10	3.55 ± 0.01	5.67 ± 0.10	3.85 ± 0.06
$g_{GeSe}^{PW}(r)$	2.41 ± 0.10	3.76 ± 0.01	5.60 ± 0.01	3.72 ± 0.03

Table 6.5. Coordination numbers as defined in section 2.4.1. Reprinted table with permission from [47]. Copyright (2009) by the American Physical Society.

	n_{Ge}	n_{Se}	n_{ave}
BLYP	3.77 ± 0.02	2.11 ± 0.02	2.66 ± 0.02
PW	3.80 ± 0.02	2.25 ± 0.02	2.77 ± 0.02
exp [6]	3.75 ± 0.3	1.98 ± 0.15	2.57 ± 0.2

approaching $g_{GeGe}^{exp}(r)$ than $g_{GeGe}^{PW}(r)$. An interesting feature proving better agreement with experiments is the shoulder in the main peak of $g_{GeGe}^{BLYP}(r)$, found at 3.1 Å, reflecting the presence of edge-sharing connections among tetrahedra. Turning to the Ge–Se pair correlation functions, we notice that the BLYP scheme is capable of reproducing the height of the first peak and the sharp decay down to very small values. There is a marked improvement on the value of neighbors in the first shell of coordination (3.55, BLYP; 3.50, experiments, 3.76, PW, see table 6.4).

Our analysis can be continued by looking in table 6.5 at the coordination numbers defined in section 2.4.1. In the case of the PW data, the underestimated value of n_{Ge}^{Ge} was compensated by the overestimate of n_{Ge}^{Se} producing a somewhat artificial agreement for n_{Ge}. In the BLYP case, one has close values for the three contributions n_{Ge}^{Ge}, n_{Se}^{Se} and n_{Ge}^{Se}. As a result, the calculated and experimental average coordination numbers n_{ave} are within 3.5 %. To conclude this analysis, it appears that BLYP improves upon PW by providing a better short-range structure for liquid $GeSe_2$, as illustrated by a more structured first shell of Ge neighbors and, globally, $g_{GeGe}(r)$ in much better agreement with neutron scattering data.

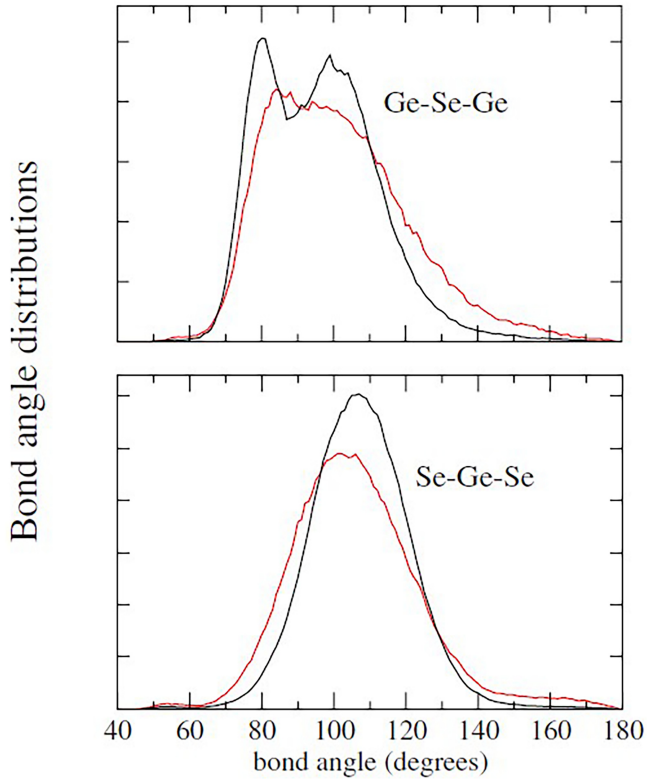

Figure 6.23. Bond-angle distributions Ge–Se–Ge (top) and Se–Ge–Se (bottom). Black line: BLYP results [47], red line: PW results [7]. Reprinted figure with permission from [47]. Copyright (2009) by the American Physical Society.

The same ideas can be further appreciated by showing the distribution θ_{SeGeSe} and θ_{GeSeGe} of the Se–Ge–Se and Ge–Se–Ge bond angles, respectively. θ_{SeGeSe} and θ_{GeSeGe} includes neighbors within less than 3 Å (figure 6.23). An improved tetrahedral order manifests itself via the shape of θ_{SeGeSe}(BLYP) that becomes symmetric around 109° with a higher intensity. Also, focusing on θ_{GeSeGe}(BLYP) for values in between 80° and 100°, there are now two discernible peaks instead of a flat maximum. This means that θ_{GeSeGe}(BLYP) results from two contributions, due to edge-sharing connections between tetrahedra (around 80°) and corner-sharing connections between tetrahedra (around 100°). These features are indications of enhanced tetrahedral organization by confirming all previous conclusions drawn on the basis of the pair correlation functions and the coordination numbers.

6.7.4 Liquid $GeSe_2$: BLYP vs PW, reciprocal space and intermediate range properties

We have seen that the BLYP approach for the XC functional is able to improve the short-range properties of liquid $GeSe_2$ by confirming that proper localization of valence electrons is a crucial property to achieve improved agreement with experiments. While

applying first this 'localization' recipe (from LDA to GGA, see section 3.6.5), we made substantial progresses for both short and intermediate range properties. Is this also the case when BLYP is employed instead of the first GGA adopted, namely PW? Figure 6.24 provide some hints in this context, at least if one is willing to rely on BLYP to obtain a marked step forward in terms of intermediate range properties, such as the FSDP intensity in $S_{CC}(k)$. One notices that the performances of BLYP and PW are overall similar for $S_{NN}(k)$ and $S_{NC}(k)$, some differences being hard to ascribe to the choice of the model since minimal and comparable to the extent of statistical errors. The same holds for $S_{CC}(k)$, in which only small shoulder appears at the FSDP location, proving that the experimental peak is underestimated in both PW and BLYP approaches.

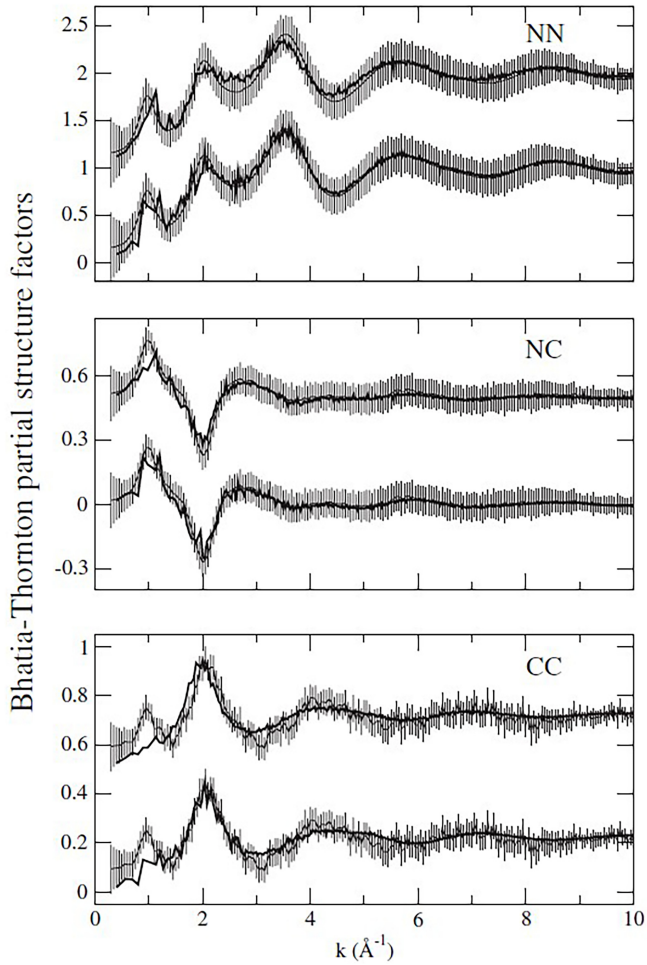

Figure 6.24. Bhatia–Thornton partial structure factors for liquid $GeSe_2$. In each panel, the experimental results of [6] are compared with the BLYP calculations [47] (bottom part) and with the PW calculations [7] (top part). $S_{NN}(k)$, $S_{NC}(k)$ and $S_{CC}(k)$ obtained within the PW scheme have been shifted up by 1, 0.6, and 0.5, respectively. Reprinted figure with permission from [47]. Copyright (2009) by the American Physical Society.

Therefore, we can conclude that the BLYP generalized gradient approximation has an undeniable effect on the short-range properties but it is much less impactful on the side of the intermediate range ones. When these results where obtained (2009) we were quite confident that the use of other XC functionals might have brought the desired improvements on the intermediate range properties. In view of what has been obtained since then, we have to admit that this kind of search has not ended yet, partially because other valuable goals have been identified leading us to postpone or reconsider the strategy needed to settle this open issue.

6.7.5 Liquid $GeSe_2$: BLYP vs PW, dynamical properties

Another way of monitoring the sensitivity of structural properties to the details of the atomic-scale model consists in calculating the diffusion coefficients. On an intuitive basis, the tetrahedra are very much stable in a network that is chemically ordered since there is a little mobility when atoms are arranged in structural units consistent with the optimal atomic bonding character (the valence) or, in terms of charges, with their positive or negative state. On the other hand, if there are departures from chemical order (as it can occurs in a AX_2 network with homopolar bonds and miscoordinations), mobility increases since the network rearranges in the search of more favorable arrangements through changes in the bonding coordination. In section 3.3 we had mentioned an example of correlation between the values of the diffusion coefficients and the atomic structure worth referring to again here. A comparison carried out between structures of liquid $GeSe_2$ obtained via FPMD and a polarizable ionic model (PIM) (see [13]) based on point charges was instrumental to highlight the drastic differences between networks allowing (FPMD) or hampering (PIM), due to stringent physical reasons, departures from chemical order. Within the PIM model, the diffusion coefficient is as low as $10^{-6}\,cm^2\,s^{-1}$ at $T = 3000$ K, while they are much larger even at $T = 1050$ K for the FPMD model, as made explicit in [13] (see section 3.3). Since we have seen that the tetrahedral order is larger in the BLYP model than in the PW one for liquid $GeSe_2$ at $T = 1050$ K, the question arises on whether this corresponds to diffusion coefficients larger in PW than in BLYP, for which chemical order is higher. The comparison between the calculated statistical average of the mean-square displacement displacement

$$\langle r_\alpha^2(t)\rangle = \frac{1}{N_\alpha}\left\langle \sum_{i=1}^{N_\alpha} |\mathbf{r}_{i\alpha}(t) - \mathbf{r}_{i\alpha}(0)|^2 \right\rangle \tag{6.7}$$

for both species, Ge and Se, obtained within the PW and the BLYP schemes, is shown in figure 6.25, with the diffusion coefficients obtained in the infinite time limit as

$$D_\alpha = \frac{\langle r_\alpha^2(t)\rangle}{6t}. \tag{6.8}$$

One obtains values for the BLYP calculations equal to $2\times10^{-6}\,cm^2\,s^{-1}$ for both species. These values are definitely smaller than the PW values ($2.2\times10^{-5}\,cm^2\,s^{-1}$ for

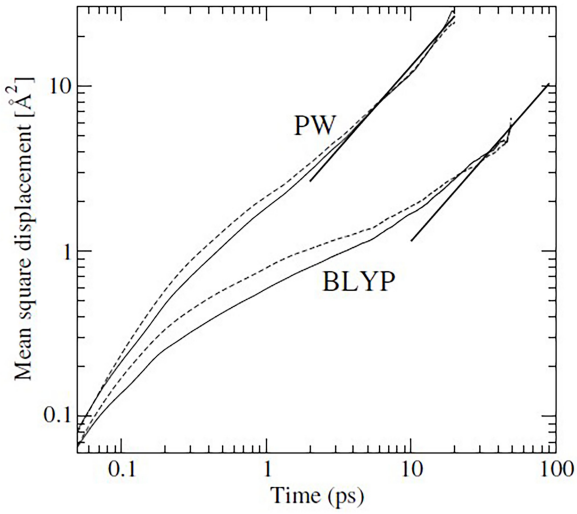

Figure 6.25. Average mean-square displacements for Ge (dashed line) and Se atoms (full line of liquid $GeSe_2$). The infinite time behavior corresponding to a slope equal to 1 in the log–log plot of $<r_\alpha^2(t)>$ vs t is also shown. Reprinted figure with permission from [47]. Copyright (2009) by the American Physical Society.

both Ge and Se) and in much better agreement with the experimental estimate (4.5×10^{-7} cm^2 s^{-1}, see [47] for details on the physical foundations of this comparison). Therefore, atomic mobility reflects well the changes in the atomic structure that remains, most likely, moderately too disordered in terms of chemical bonding. This was expected in view of the difference persisting at the level of Ge–Ge correlations in both the short and, to a larger extent, the intermediate range properties.

6.7.6 Glassy $GeSe_2$: BLYP vs PW and further thoughts

In a short paper appeared in 2010 [48], we tried to extend the above rationale to the case of glassy $GeSe_2$, by assuming that the same considerations developed for the liquid hold for a system obtained from it via rapid quench. While we found some improvements in the structural properties when compared to experiments (in particular, for the number of Ge–Ge homopolar bonds), nothing striking came up in terms of a clear-cut set of changes approaching the BLYP result to experiments. The comparison was based on a single trajectory and could not be considered conclusive. Despite the limits affecting that analysis, we obtained a further indication of the tendency toward more structured shells of Ge neighbors inherent in BLYP while the main peak remained quite small in intensity when compared to experiments. Ever since the discovery of the improved structural features obtained when using BLYP on $GeSe_2$ disordered systems, this scheme has been adopted to model other chalcogenides, even though other comparison with different XC choices were made in some cases, as glassy $GeSe_4$. We shall focus on some of these results in the next chapters.

References

[1] Salmon P S 1994 *Proc. R. Soc. Lond.* A **445** 351
[2] Vashishta P, Kalia R K, Antonio G A and Ebbsjö I 1989 *Phys. Rev. Lett.* **62** 1651–4
[3] Vashishta P, Kalia R K and Ebbsjö I 1989 *Phys. Rev.* B **39** 6034–47
[4] Iyetomi H, Vashishta P and Kalia R K 1991 *Phys. Rev.* B **43** 1726–34
[5] Petri I, Salmon P S and Fischer H E 2000 *Phys. Rev. Lett.* **84** 2413–6
[6] Penfold I T and Salmon P S 1991 *Phys. Rev. Lett.* **67** 97–100
[7] Massobrio C, Pasquarello A and Car R 2001 *Phys. Rev.* B **64** 144205
[8] Massobrio C and Pasquarello A 2008 *Phys. Rev.* B **77** 144207
[9] Waseda Y 1980 The structure of non-crystalline materials *Liquids and Amorphous Solids* (New York: McGraw-Hill)
[10] Bhatia A B and Thornton D E 1970 *Phys. Rev.* B **2** 3004–12
[11] Salmon P S 1992 *Proc. R. Soc. Lond.* A **437** 591
[12] van Roon F H M, Massobrio C, de Wolff E and de Leeuw S W 2000 *J. Chem. Phys.* **113** 5425–31
[13] Wilson M, Sharma B K and Massobrio C 2008 *J. Chem. Phys.* **128** 244505
[14] Susman S, Volin K J, Montague D G and Price D L 1990 *J. Non-Cryst. Solids* **125** 168–80
[15] Salmon P S and Petri I 2003 *J. Phys.: Condens. Matter* **15** S1509–15
[16] Massobrio C, van Roon F H M, Pasquarello A and De Leeuw S W 2000 *J. Phys.: Condens. Matter* **12** L697
[17] Petri I, Salmon P S and Spencer Howells W 1999 *J. Phys.: Condens. Matter* **11** 10219
[18] Elliott S R 1991 *Phys. Rev. Lett.* **67** 711–4
[19] Moss S C and Price D L 1985 Random packing of structural units and the first sharp diffraction peak in glasses *Physics of Disordered Materials. Institute for Amorphous Studies Series* ed D Adler, H Fritzsche and S R Ovshinsky (Boston, MA: Springer)
[20] Price D L, Moss S C, Reijers R, Saboungi M L and S Susman 1988 *J. Phys. C: Solid State Phys* **21** L1069–72
[21] Elliott S R 1992 *J. Phys.: Condens. Matter* **4** 7661–76
[22] Busse L E and Nagel S R 1981 *Phys. Rev. Lett.* **47** 1848–51
[23] Bridenbaugh P M, Espinosa G P, Griffiths J E, Phillips J C and Remeika J P 1979 *Phys. Rev.* B **20** 4140–4
[24] Phillips J C 1981 *J. Non-Cryst. Solids* **43** 37–77
[25] Wilson M and Madden P A 1994 *Phys. Rev. Lett.* **72** 3033–6
[26] Gaskell P H and Wallis D J 1996 *Phys. Rev. Lett.* **76** 66–9
[27] Wilson M and Madden P A 1998 *Phys. Rev. Lett.* **80** 532–5
[28] Sarnthein J, Pasquarello A and Car R 1995 *Phys. Rev.* B **52** 12690–5
[29] Luchnikov V A, Medvedev N N, Appelhagen A and Geiger A 1996 *Mol. Phys.* **88** 1337–48
[30] Corti D S, Debenedetti P G, Sastry S and Stillinger F H 1997 *Phys. Rev.* E **55** 5522–34
[31] Sarnthein J, Pasquarello A and Car R 1995 *Phys. Rev. Lett.* **74** 4682–5
[32] Massobrio C, Pasquarello A and Car R 1998 *Phys. Rev. Lett.* **80** 2342–5
[33] Massobrio C and Pasquarello A 2007 *Phys. Rev.* B **75** 014206
[34] Massobrio C, Celino M and Pasquarello A 2003 *J. Phys.: Condens. Matter* **15** S1537
[35] Rowlands R F, Zeidler A, Fischer H E and Salmon P S 2019 *Front. Mater* **6**
[36] Haye M J, Massobrio C, Pasquarello A, De Vita A, De Leeuw S W and Car R 1998 *Phys. Rev.* B **58** R14661–4
[37] Celino M and Massobrio C 2003 *Phys. Rev. Lett.* **90** 125502

[38] Celino M and Massobrio C 2002 *Comput. Mater. Sci.* **24** 28–32
[39] Price D L, Saboungi M-L and Barnes A C 1998 *Phys. Rev. Lett.* **81** 3207–10
[40] Boolchand P and Bresser W J 2000 *Philos. Mag.* B **80** 1757–72
[41] Johnson R W, Price D L, Susman S, Arai M, Morrison T I and Shenoy G K 1986 *J. Non-Cryst. Solids* **83** 251–71
[42] Massobrio C, Celino M and Pasquarello A 2004 *Phys. Rev.* B **70** 174202
[43] Perdew J P and Wang Y 1992 *Phys. Rev.* B **45** 13244–9
[44] Perdew J P, Chevary J A, Vosko S H, Jackson K A, Pederson M R, Singh D J and Fiolhais C 1992 *Phys. Rev.* B **46** 6671–87
[45] Becke A D 1988 *Phys. Rev. A* **38** 3098–100
[46] Lee C, Yang W and Parr R G 1988 *Phys. Rev.* B **37** 785–9
[47] Micoulaut M, Vuilleumier R and Massobrio C 2009 *Phys. Rev.* B **79** 214205
[48] Massobrio C, Micoulaut M and Salmon P S 2010 *Solid State Sci.* **12** 199–203
[49] Massobrio C and Pasquarello A 2001 *J. Chem. Phys.* **114** 7976